Chapter 10
Optofluidic Devices for Bioanalytical Applications

Hui Yang and Martin A. M. Gijs

10.1 Introduction

Today, we are experiencing fast changes in personal health management: from present one-fits-all post-medical care to targeted therapy based on genetics or molecular mechanisms in different time frames (Hamburg & Collins, 2010). Accordingly, the major task of analytical techniques in biological research now relies on detecting, diagnosing, and monitoring molecular dynamics in terms of pathology and physiology, which will benefit early diagnosis, prognosis, and disease monitoring (Jung & Lee, 2015). Therefore, the most pivotal step is generating a customized system that can track the temporal/spatial distribution of targeted molecules or interrogate their behavior in cellular/subcellular level.

To meet with such challenges, in recent years, optofluidic technology has drawn much focuses. Optofluidics, namely, bridging "optics" and "microfluidics," is capable of manipulating light with on-chip fluidic processes, or using light to control fluidic entities. However, recent efforts on optofluidics have already pushed the technology forward and exceeded its original definition, and either (1) using fluidic and optical elements synergistically or (2) employing advanced optical/photonic methods on microfluidics platform to concretize enhanced deployment, reliability, accuracy, throughput, especially in the on-chip aspect, can be defined as optofluidics (Minzioni et al., 2017; Chen et al., 2019; Yang et al., 2019). Over the last two decades, a fast growing interest was noticed for developing microdevices that

H. Yang (✉)
Bionic Sensing and Intelligence Center, Institute of Biomedical and Health Engineering, Shenzhen Institutes of Advanced Technology, Chinese Academy of Sciences, Shenzhen, China
e-mail: hui.yang@siat.ac.cn

M. A. M. Gijs
Laboratory of Microsystems, École Polytechnique Fédérale de Lausanne, Lausanne, Switzerland

Z. Yang (ed.), *Advanced MEMS/NEMS Fabrication and Sensors*,
https://doi.org/10.1007/978-3-030-79749-2_10

integrate one or several functionalities (e.g., sample preparation, reaction, separation, and detection) onto a single chip, the latter being of only millimeter-size up to a few square centimeters in size (Haeberle & Zengerle, 2007; Yang & Gijs, 2018; Manz et al., 1990). These microdevices can be used either to perform a certain type of chemical analysis or, more generally, for other nonanalytical lab processes like sample pre-treatment, and they are known as "micro total analysis systems (μTAS)" or "lab-on-a-chip (LOC)" devices. The concept of the integrated μTAS or LOC microfluidic device was introduced by Manz et al. in the early 1990s (Mark et al., 2010). Since then, microfluidic devices have led to great advances in many research fields. Benefiting from microfluidics such as low consumption, micro−/nanoscale sample manipulation, compatibility with consumer electronics, and optofluidic devices that integrate microfluidics with high-end micro-optical components and methods offers various scenarios in bioanalytical applications and personalized medicine (Jung & Lee, 2015).

In this chapter, we focus on recent developments in the realization and use of micro-optical components that are directly integrated onto a microfluidic device. We introduce basic working principles of micro-optics (Sect. 10.2), and optofluidic components and integrated systems (Sect. 10.3). In Sect. 10.4, we will give a brief overview of the microfabrication technologies for realization of microfluidic devices and micro-optical components. Subsequently, optofluidic devices that eventually have been used for a full bioanalytical application (Sect. 10.5) will be presented. We will conclude by explaining the advantages of optofluidic systems for tackling analytical problems in general and highlighting the advantages of different micro-optical components specifically. We hope that the chapter provides the reader with some orientation in the field and enables selecting platforms with appropriate characteristics for his/her application-specific requirement.

10.2 Fundamentals on Micro-Optics

Based on basic optical principles, one can classify micro-optical components into (1) refractive optical components that rely on the change of the refractive index at an interface, such as lenses, prisms, and mirrors; (2) diffractive optical structures that enable shaping of an optical beam by diffractive/interference effects, such as diffraction gratings; and (3) hybrid (refractive/diffractive) structures. Refractive and diffractive optical components share many similarities when they are used to manipulate monochromatic light, but their response to broadband light is very different. For a material with normal dispersion, refractive lenses have larger focal distances for red light than for blue light, and prisms deflect longer wavelengths by a smaller angle; the contrary occurs for diffractive lenses and gratings. This contrasting behavior arises because two different principles are used to shape the light: refractive optics relies on the phase that is gradually accumulated through propagation, while diffractive optics operates by means of interference of light transmitted through an amplitude or phase mask. The decision to use diffractive or refractive

optics for a specific optical problem depends on many parameters, e.g., the spectrum of the light source, the aimed optical application (beam shaping, imaging, etc.), the efficiency required, the acceptable stray light, etc. Arbitrary wavefronts can be generated very accurately by diffractive optics. A drawback for many applications is the strong wavelength dependence. Diffractive optics is therefore mostly used with laser light and for nonconventional imaging tasks, like beam shaping, diffusers, filters, and detectors. Refractive optical elements have in general higher efficiency and less stray light, even though in some cases it is more difficult to make refractive lenses with precise focal lengths or aspheric shapes. Moreover, for broadband applications, diffractive optical elements (DOEs) can be combined with refractive optics to correct for the chromatic aberration. This combination allows systems with low weight or which consist of only one material. We summarize in the following fundamental optical principles like light reflection and refraction, light wave interference, diffraction, and polarization.

From a physics point of view, a *light wave* is an oscillatory electric and magnetic field that co-propagate through space. The electric and magnetic field components of this electromagnetic radiation are oscillating in phase perpendicular to the propagation direction and with respect to each other. Optical methods make use of electromagnetic radiation with wavelengths from ~200 nm to a few μm. This interval can be subdivided into the ultraviolet (UV) region (~200–400 nm), the visible (Vis) region (~400–700 nm), and the near-infrared (NIR) region (~700 nm to a few μm). The UV/Vis region is used most widely for microsensing systems, especially in fluorescence detection methods, but also in absorbance and chemiluminescence techniques. When the amplitude of electromagnetic waves composing a light beam oscillates in the same plane, the light is said to be polarized. Polarized light is generally classified into two groups depending on how the electric waves are aligned with the plane of incidence onto a dielectric surface. The plane of incidence is the plane composing the incident, reflected, and transmitted rays. Transverse magnetic (TM), parallel (//), P, and O are all notations to refer to waves that are polarized such that the electric field is in the plane of incidence. Transverse electric (TE), perpendicular (⊥), S, and E are all ways to refer to polarization perpendicular to the plane of incidence. The polarization of light can affect many aspects of optical systems, and materials can have different properties for different polarizations, such as indices of refraction or reflectivity.

Reflection of light happens when light is incident on an interface between two transparent optical media. How light reflects from a surface is governed by the law of reflection: the angle that the reflected ray makes with the normal at the point of incidence is always equal to the angle the incident ray makes with the same normal; the incident ray, reflected ray, and normal always lie in the same plane. The behavior of reflection can also be shown by Fermat's principle, which states that light will take path with the shortest travel time to go from one point to another. Therefore, depending on the incident angle of the light onto a surface, light will only reflect at an angle that is the same as the incident angle, i.e.,

$$\theta_{\mathrm{i}} = \theta_{\mathrm{o}} \tag{10.1}$$

Scattering can also change the direction of propagation of a light beam. An incident wave can be scattered by a diffusely reflecting surface that generates scattered waves into various directions. A wave can also be scattered while propagating through a diffuse liquid or solid medium with a distribution of refractive indices.

Refraction is the bending of light waves at an interface between two media with different optical density. These two transparent optical media are distinguished from one another by the index of refraction n. The relation between the sines of the angles of incidence and refraction and the indices of refraction of the two media is defined by Snell's law:

$$n_{\mathrm{i}} \sin\theta_{\mathrm{i}} = n_{\mathrm{r}} \sin\theta_{\mathrm{r}} \tag{10.2}$$

Total internal reflection can occur when light in a high-index medium reaches a low-index medium ($n_{\mathrm{i}} > n_{\mathrm{r}}$). When $\theta_{\mathrm{r}} = 90°$, the corresponding incident angle is called the critical angle. Ideally, any incident ray at the critical angle or higher will cause total internal reflection. Although all of the incident energy is reflected, the solution of Maxwell's equations predicts the existence of an electromagnetic field in the less dense medium with intensity decaying exponentially away from the interface. This evanescent wave propagates parallel to the interface and has a decay length, i.e., penetration depth d, on the order of the wavelength of the illumination light λ_{i}. The evanescent intensity field is described by the following set of equations:

$$I(z) = I_0 e^{-z/d} \tag{10.3}$$

$$d = \frac{\lambda_{\mathrm{i}}}{4\pi}\left[n_{\mathrm{i}}^2 \sin^2\theta_{\mathrm{i}} - n_{\mathrm{r}}^2\right]^{-\frac{1}{2}} \tag{10.4}$$

where z is the transverse dimension, $I(z)$ is the intensity of the evanescent field throughout the medium with lower refractive index, I_0 is the intensity at the interface of two media (at $z = 0$), θ_{i} is the angle of incidence, n_{i} is the refractive index of the incident medium, and n_{r} is the refractive index of the secondary medium. The penetration depth usually ranges between 30 and 300 nm. The polarization of the incident beam does not affect the penetration depth, but it does affect the amplitude of the evanescent field. When the incident angle equals the critical value at which $n_{\mathrm{i}}^2 \sin^2\theta_{\mathrm{i}} - n_{\mathrm{r}}^2 = 0$, d goes to infinity and the refracted light propagates along the surface; therefore, the incident angle θ_{i} must be greater than the critical angle $\theta_{\mathrm{c}} = \mathit{arcsin}\,(n_{\mathrm{r}}/n_{\mathrm{i}})$ for total internal reflection to occur.

It was shown that the penetrating evanescent field could be absorbed or diverted by bringing an absorbent or a high-index material into close proximity to the reflecting surface; hence, the total reflection can be frustrated (Harrick, 1962). A classic experiment to demonstrate this phenomenon is done by using two prisms. The light is incident on the surface of the first prism condition of total internal reflection so as to generate the evanescent field, and the second prism reads this evanescent field and emits it to the far field. As the gap between two prisms decreases, the transmittance increases exponentially, except in the near-field region where the

transmittance curve deviates from an exponential decay and exhibits linear characteristics due to the strong interaction between the two prism surfaces via the evanescent field. This special characteristic associated with the frustrated total internal reflection (FTIR) has been exploited in different applications, such as near-field microscopy (Wynne et al., 2012; Carney & Schotland, 2001), optical coupling (Hanumegowda et al., 2005; Gupta & Goddard, 2013), and biochemical detection (Bruls et al., 2009; Dittmer et al., 2010). The method of FTIR was extended into a new technique after the excitation of non-radiative surface plasma waves was found in a thin metal film in contact with the prism base. The surface plasmon resonance (SPR) technique is widely used in gas detection and biosensing. By passing polarized light through a high-refractive index prism, the polarized light becomes TIR and generates an evanescent wave that penetrates the thin metal film. Monitoring the intensity of the reflected light as a function of the angle of incidence, the intensity of reflected light will pass through a minimum, as energy from the evanescent wave is absorbed by the surface plasmons in the thin metal film. The angle at which the minimum reflected light intensity occurs is known as the SPR angle. The SPR angle is sensitive to changes in the dielectric refractive index at close proximity to the metal surface (Helmerhorst et al., 2012). By immobilizing receptor molecules at the metal surface, this technique can be applied to diagnostic applications as the interaction of biomolecules will produce a change in the refractive index near the metal surface, causing a shift in the SPR angle and providing a detectable signal. Usually, the ligand of interest is attached to the surface using well-established surface chemistries, and the analyte is then passed over the ligand-derivatized matrix. Any change in mass following the interaction between the ligand and analyte is detected as a change in the angle of the incident light needed to generate the SPR phenomenon. This is measured as an energy or reflectance dip as a function of pixels, which translates to response units (RU) over time. The RU change is directly proportional to molecular mass change, and so binding kinetics and stoichiometry can be measured in real time without using labeling techniques. Snell's law also determines the imaging properties of lenses. A ray incident on the lens refracts at the front surface (according to Snell's law), propagates through the lens, and refracts again at the rear surface. The principles and working mechanisms of lenses will be introduced later.

Interference means that two or more electromagnetic waves can be combined by adding or subtracting electric and magnetic field vectors with proper attention to phase and amplitude. Two overlapping monochromatic waves are incoherent if the waves have no persistent phase relationship. In this case, the power carried by the waves is additive. On the other hand, if the fluctuations of phase and amplitude of two beams are correlated, the beams are coherent. If two monochromatic beams are coherent, propagate in essentially the same direction, are polarized in the same direction, and are in phase, then in regions of overlap, their electric vectors are added and the waves are said to interfere constructively. The power is proportional to the square of the vector sums of the electric vectors. If the waves are 180° out of phase, the vectors are subtracted, the waves interfere destructively, and if the two waves have equal power, the combined wave has no power.

Diffraction refers to the process by which a beam of light is spread out as a result of passing through a narrow aperture or across an edge. The image of a point object is not an ideal point, even when formed by a perfect optical element. This is due to the diffraction phenomenon. Diffraction sets the limit of resolution of an image. The intensity point spread function is the intensity distribution in the image that is formed from a point object. If an optical detection system is exposed to an object emitting incoherent radiation, the formed image is the superposition of the intensity point spread functions associated with all of the points that make up the object. Two points of a diffraction-limited image can be resolved when the central peak of the point spread function of one falls on the first zero of the other and the resulting pattern has two peaks with a 74% valley between them. This is the *Rayleigh criterion*. The diffraction-limited resolution of a system with a circular aperture is

$$\Delta x = 0.61\lambda / \mathrm{NA} \tag{10.5}$$

where λ is the wavelength of the light beam and NA refers to the numerical aperture of the system. The numerical aperture is an important parameter for a lens, related directly to how much light the lens gathers. The definition of numerical aperture is given as

$$\mathrm{NA} = n \sin \alpha \tag{10.6}$$

where n is the index of refraction of the intervening medium between object and lens and α is the half-angle defined by the limiting rays that are collected by the lens. The "light-gathering" power of the microscope's objective lens is thus increased by increasing the refractive index of the intervening medium. In addition, the numerical aperture is closely related to the acceptance angle of optical waveguides and fibers. For conventional optical microscopes, diffraction sets the ultimate limit of resolution of an image. The evanescent components that carry the fine information about the object decay exponentially in a medium with positive permittivity and permeability and are lost before reaching the image plane; only the propagating wave components emanating from the illuminated object can be collected at the image plane (Pendry, 2000; Fang et al., 2005).

It has been demonstrated that dielectric microspheres can be used as microlenses to achieve near-field focusing and magnification, resulting in the capability to resolve features beyond the diffraction limit (Wang et al., 2011; Yan et al., 2015). High-index microspheres (n ~ 1.9–2.1), fully immersed in liquid, actually allow enhanced imaging with minimum resolved feature sizes of ~λ/7 using white-light illumination for imaging of nano-features (Darafsheh et al., 2012) and adenoviruses (Li et al., 2013), as well as with fluorescent microscopic setup for resolving the structures of subcellular organelles (Yang et al., 2014). In these works, the microspheres were simply placed on top of the sample object, where they collected the underlying sample's near-field nano-features and subsequently transformed the near-field evanescent waves into far-field propagating waves, creating a magnified image in the far field, which is collected by a conventional optical microscope

(Wang et al., 2011; Yang et al., 2014; Yang & Gijs, 2015). The super-resolution imaging capability (i.e., imaging beyond the classical diffraction limit) of microspheres is linked to the so-called photonic nanojet phenomenon. A substantial literature has developed regarding the existence, properties, and potential applications of the photonic nanojet (Yang et al., 2015, 2016a; Chen et al., 2004; Li et al., 2005; McLeod & Arnold, 2008; Gérard et al., 2008; Heifetz et al., 2009). In principle, a photonic nanojet is a narrow light beam with high optical intensity that can be generated by a transparent dielectric symmetric body, like a microcylinder or microsphere, upon illumination. The nanojet that emerges from a microsphere is located in the immediate vicinity of the rear surface of the sphere. It is a nonresonant phenomenon that appears for microspheres with a diameter of the order of 10–100λ and with a ratio of their refractive index nms to the refractive index of the mostly water-based background medium nw that is smaller than about 2. The nanojet can maintain a subwavelength full-width-at-half-maximum (FWHM) transverse beam width along a path that can extend more than ~2λ beyond the sphere, and the minimum FWHM beam width can be smaller than the classical diffraction limit, in fact as small as ~λ/3. The next section introduces the field of optofluidics, from typical components to its applications.

10.3 Optofluidic Components and Integrated Systems

From an engineering point of view, optical detection in chemical/biochemical microfluidic devices is easily implemented via incorporation of optical components, such as light sources, waveguides, microlenses, and detectors, to achieve a fully operational micro-optical system. Along with the development of microfluidic technologies, researchers also improve lab-on-a-chip functionalities by incorporating optical components into the same system (Monat et al., 2007). Most solid-phase optical components are lack of capability on deformation and position adjustment, as they are usually fixed in an integrated system. On the contrary, fluid-based optical components can achieve self-tunability, adaptivity, and precise alignment in the context of optofluidic circuits. In the following years, the number of papers regarding to "optofluidics" has been booming with a wide variety of applications, such as biochemical sensor (Fan et al., 2008), bio-imaging (Cui et al., 2008), energy production and harvesting (Erickson et al., 2011), on-chip manipulation of cells (Huang et al., 2014; Yang et al., 2016b), etc. Many research groups have presented a large collection of optofluidic components for imaging. These optofluidic components are categorized in terms of either their working mechanisms or their functions similar to their macro-scale counterparts (e.g., waveguide, lens, cavity, etc.) (Song & Tan, 2017; Zhao et al., 2013). We will present the working principles of these optofluidic components, and focus on their timely progresses and challenges in this section.

10.3.1 Optofluidic Light Source

Light sources can be applied in microfluidic systems through free-space coupling or by direct integration on-chip. Commercial light-emitting diodes (LEDs) have been widely used as light sources in hybrid assembled devices. However, an optofluidic chip requires synergetic combination between the microfluidic device and micro-optical system. Organic light-emitting diodes (OLEDs) and dye lasers are currently the two most used integrated light sources on microfluidic chips (Yao et al., 2005; Li & Psaltis, 2008). The advantages of these two devices are that they can be fabricated on the same substrate as the microfluidic system and readily integrated with other fluidic functionalities. They can also benefit from the fluidic scheme: liquid OLEDs can allow realization of truly flexible displays without detachment of the liquid-emitting layer from the electrodes (Xu & Adachi, 2009); the problem of OLED degradation resulting from the decomposition of organic materials no longer exists as the liquid emitters can be refreshed by a flow (Kasahara et al., 2013); and the characteristics of dye lasers are amenable to tuning by changing the dye solution (Li & Psaltis, 2008).

The light sources are usually used together with other micro-optic components to generate an optofluidic laser. The first-generation optofluidic laser based on a Fabry-Pérot resonator was developed by Whitesides' group (Vezenov et al., 2005). In this work, fluorescence was constrained in the core flow of an optofluidic waveguide. Both ends of the waveguide were coated with a thin layer of gold, acting as reflecting mirrors. Therefore, the fluorescence bounced back and forth and escaped from the gold layer, forming a laser. This laser system is configurable in the aspects of emission wavelength, numerical aperture, and absorbance by changing dye/solvent composition and flow rates of core/cladding layer. An optofluidic laser based on distributed-feedback (DFB) gratings was proposed (Song et al., 2009). As shown in Fig. 10.1a, a SU-8 pattern with high-refractive index (i.e., DFB resonator) is sandwiched between a cladding flow and a silicon dioxide layer. The DFB grating has relatively large surface area and allows enhanced interaction of the evanescent tail

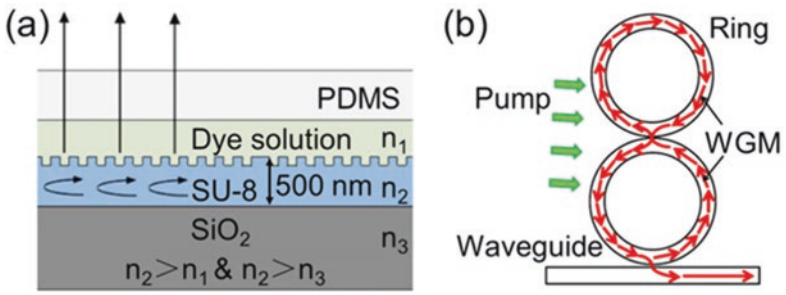

Fig. 10.1 (**a**) DFB resonator-based optofluidic laser. (**b**) Optofluidic ring resonator laser. (Reproduced with permission (Chen et al., 2019), Copyright 2019, Optical Society of America)

with the upper liquid gain medium, forming a surface-emitting optofluidic laser via output coupling.

Though single-mode operation and large tunable wavelength range have been realized with the above two types of optofluidic lasers, the relative low Q factors (~1e3) prevent them from achieving low lasing threshold (Fan & White, 2011). As a comparison, an optofluidic ring resonator (OFRR) laser system can achieve high Q factor; the schematic is shown in Fig. 10.1b. The system consists of two mismatched ring resonators and a liquid-filled waveguide (Lee et al., 2011). The lower ring is optically coupled with the straight waveguide but physically disconnected. Water-based medium with fluorescent dye is filled inside the structures. Upon excitation, fluorescent light is confined in the gain medium because of the polydimethylsiloxane (PDMS) sidewalls with low-refractive index, and emits through the waveguide. The optical coupling between two OFRRs and the waveguide achieves side mode suppression and a Q factor of ~1e8. To date, ring resonators have been exploited in many formats, such as microdroplets (Tang et al., 2009), microknots (Jiang et al., 2007), and microcapillaries (Shopova et al., 2007), providing an excellent optical feedback for low-threshold lasing.

10.3.2 Optofluidic Prism

How to achieve an accurate alignment among multiple optical components is one of the main challenges when designing an optofluidic system. The use of an optofluidic prism to manipulate light path would greatly alleviate such integration issue. A configurable optofluidic prism was reported (Xiong et al., 2011). By converging three laminar flow streams in a triangular-shaped chamber, the apex angle of the prism can be adjusted by altering flow rates. Thus, one can steer optical path in-plane due to light refraction at the interface of two fluids. Further explorations on optofluidic prisms focus on system rotatability and optical scanning robustness. Zappe's group developed a 360° rotatable optofluidic prism which enabled rotational beam scanning in 16 discrete steps (Fig. 10.2) (Kopp et al., 2016). A cylindrical fluidic chamber comprising of two immiscible liquids is wrapped with flexible polymeric foils. Segmented electrodes are embedded in the foils. Upon applying variable voltages over the electrodes, local contact angle of the liquid interface can be changed due to electro-wetting effect. In this device, the total number of beam positions is determined by the number of electrodes, meaning that more meticulous beam rotation can be achieved by using more discrete electrodes.

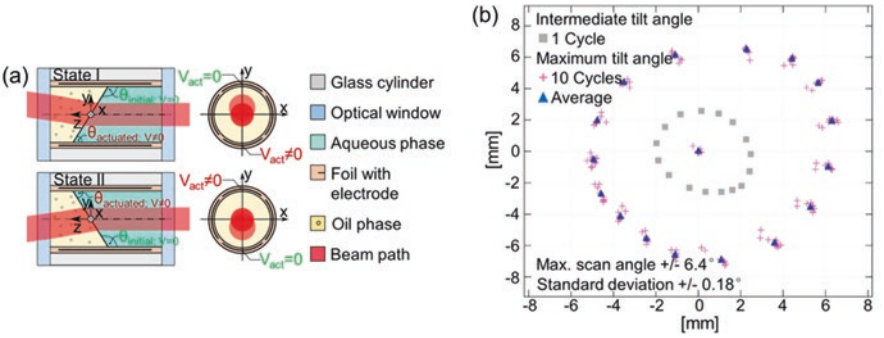

Fig. 10.2 (**a**) Rotatable optofluidic prism with beam positions tuned by electro-wetting effect. (**b**) Beam positions of the tunable prism for ten repeated cycles. Maximum tilt angle (pink crosses), spatial average (blue triangles), and smaller tilt angle (gray squares) are shown in the figure. (Reproduced with permission (Chen et al., 2019), Copyright 2019, Optical Society of America)

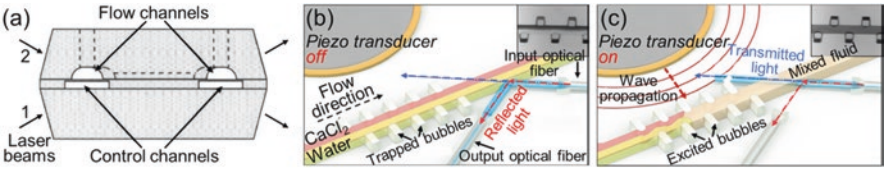

Fig. 10.3 (**a**) Schematic on a three-layer optofluidic switch with four optical facets. The arrows show the directions of both incident and reflected/transmitted laser beams. (**b**, **c**) Working mechanism of an acoustic-driven optofluidic switch without (**b**) and with (**c**) acoustic excitation. (Reproduced with permission (Chen et al., 2019), Copyright 2019, Optical Society of America)

10.3.3 Optofluidic Switch

As an important part of an optofluidic system, optical switches can modify light path and intensity (Pang et al., 2012; Campbell et al., 2004). A 2 × 2 optofluidic switch based on total internal reflection was proposed by Campbell et al. (2004). The device was fabricated using soft lithography, consisting of two distinct layers which are separated by a thin PDMS membrane with low Young's modulus (Fig. 10.3a). The upper layer is a fluidic layer containing a mirror channel with two inlets (one for low-refractive index medium and the other for high-refractive index medium), and the lower layer is a control layer containing five pneumatic valves. These valves are used to control the exchange of sample media in the mirror channel. Upon illumination, the light beam can be transmitted or reflected by tuning the refractive index of the medium in the mirror channel. Huang's group developed an acoustic-driven optofluidic switch (Huang et al., 2012). This device consists of a microfluidic channel that is sandwiched between air-filled cavities in PDMS. Deionized water (n = 1.33) and $CaCl_2$ solution (n = 1.42) are introduced in the main channel. Incident laser beam is reflected at the interface between PDMS (n = 1.41) and DI water when the piezoelectric transducer is turned off (Fig. 10.3b).

On the contrary, the oscillated cavities mix the two media when the transducer is turned on, and the incident laser beam is transmitted through the microchannel since the refractive index of the mixed solution is close to that of PDMS (Fig. 10.3c).

10.3.4 Optofluidic Waveguide

An optical waveguide is a physical structure that transmits light along its axis, which is generally composed of a core with a cladding part. A planar optical waveguide is a waveguide fabricated in a flat format and is particularly interesting to combine with a microfluidic chip. A waveguide is a key optical element for integrated optofluidics, and has the same importance for directing light as the fluidic channel has for directing fluids. The waveguides that have been assembled on microfluidic chips rely on either total internal reflection (TIR) or wave interference for confinement of optical beams (Schmidt & Hawkins, 2008; Hawkins & Schmidt, 2008). TIR-based waveguides are composed of a high-refractive index core material surrounded with a low-refractive index cladding material. A light ray that is incident on the core-cladding interface at an angle above the critical angle of TIR propagates along the longitudinal direction. The requirement for the refractive index of the core to be bigger than that of cladding layer is easy to fulfill in solid-state devices, but poses difficulties for optofluidics. This is because the index of the solid materials used for microfabrication in both polymer- and silicon-based approaches (1.4–3.5) is larger than the index of water and most aqueous solutions (~1.33). Building TIR-based optofluidic systems requires creativity in structural design or using alternate materials. Another approach to waveguiding is the use of wave interferences to confine an optical wave. In this case, multiple layers of material are used as the waveguide cladding. These layers create multiple reflections of the electric field that can interfere constructively or destructively. The key idea is that near-perfect reflection into the original medium can be achieved even if that medium (e.g., water) has a lower refraction index than all of the cladding layer materials (e.g., silicon dioxide, silicon nitride, and titanium dioxide) (Testa et al., 2010).

A typical method for creating integrated optofluidic waveguides with TIR confinement is developed by flowing two or more different laminar liquid streams with different refractive indices inside a fluidic channel, and these streams work as core or cladding. This type of waveguide is referred to as liquid-core/liquid-cladding (L^2) waveguide. The index of the cladding liquid is smaller than that of the core liquid so that the light is guided in the channel by TIR occurring at the interface of the liquids. This concept was first demonstrated using $CaCl_2$ ($n = 1.445$) and water ($n = 1.33$) as core and cladding liquids, respectively, flowing in PDMS ($n = 1.4$) channels (Wolfe et al., 2004, 2005; Brown et al., 2006). Core fluid is first injected into the central channel through a tapered channel. Cladding fluid is then injected on either side of the central channel, resulting in the core fluid being surrounded by cladding fluid on the left and right and PDMS above and below. By changing the flow rates of the liquids, the size and the direction of the waveguides can be reconstructed. Lee et al.

developed a 3D microfluidic L^2 waveguide in which the liquid core was hydrodynamically focused in the center of the PDMS microchannel by the cladding fluids; therefore, the core liquid was not in contact with the channel walls, and this method could be used to decrease the optical loss at the top and bottom interfaces of core and channel walls (Lee et al., 2010). The performance of the L^2 waveguides is affected by the sensitivity of the stream interface to vibrations and diffusion effects. However, compared to solid-state waveguides, the L^2 waveguides show the following advantages: (1) the optical performance is tunable by controlling the fluidic properties and (2) the smooth interfaces between the core and cladding streams minimize optical loss. It has also been shown that the L^2 waveguides can be integrated with biosensing devices. Rosenauer et al. presented a liquid-core/liquid-twin-cladding waveguide for on-chip fluorescence spectroscopy (Rosenauer & Vellekoop, 2009a). The waveguide included an inner and an outer cladding fluid surrounding the core fluid. The analyte was suspended in the inner cladding fluid and excited by the evanescent wave at the fluid interface between the core and the inner cladding fluid (Fig. 10.4). Considerable reduction in sample volume and a low background noise were obtained by tuning the ratios of the flow rates of three different liquids.

10.3.5 Optofluidic Lens

A microlens is an important and key optical component for focusing and collimating light in a microfluidic optical detection system. The motivation for integration of microlenses in microfluidic devices is typically to improve the detection, e.g., by focusing the light in the channel to increase the excitation power for optical measurements (Yang et al., 2015; Schwartz et al., 2010). A microlens can be made of a hard solid surface (e.g., a microsphere) or a deformable interface such as formed

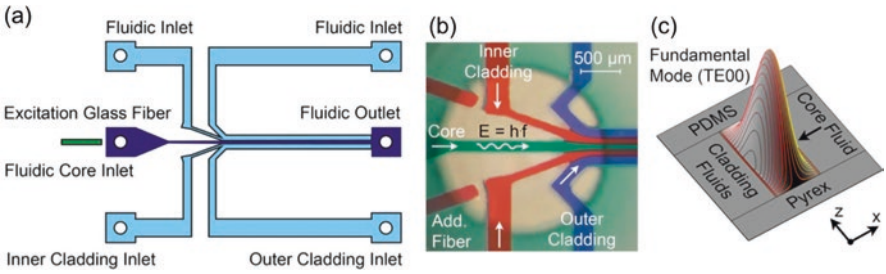

Fig. 10.4 (**a**) Schematic of an optofluidic fluorescence waveguide. (**b**) Micrograph of the L^2 waveguide structure. The hydrodynamic focusing of the core and inner cladding fluids is shown with different stained aqueous ink solutions. (**c**) Simulations from COMSOL show the fundamental mode of the waveguide; the height data expresses the normalized time-average power flow. (Reproduced with permission (Rosenauer & Vellekoop, 2009a), Copyright 2009, American Institute of Physics)

between a soft solid and a liquid, a liquid and a liquid, etc. The solid-state lenses on-chip are usually with fixed focal length, while the optical axis of the lens is vertical to the chip plane, focusing light to the channel from a top or bottom surface (Yang et al., 2015; Schwartz et al., 2010; Yang & Gijs, 2013). This type of lens is most often assembled in hybrid systems. Another type of solid lens has an optical axis parallel to the chip plane, introducing light from the sidewall of the chip (Seo & Lee, 2004; Ro et al., 2005), and can be directly fabricated on-chip. These microlenses are robust, vibration-resistant, and simple to arrange in an array of solid microlenses of specific focal lengths. Other promising and popular microlenses on-chip utilize the curvature formed by the interface between two liquids, between a liquid and a soft solid, or between liquid and air. Such microlenses are also called optofluidic microlenses, and they are dynamic optical elements and their focal lengths can be easily tuned by changing fluid characteristics, such as the type of material, concentration, and flow rate (Mao et al., 2007; Rosenauer & Vellekoop, 2009b). The major advantages of these interface-based microlenses are that they are reconfigurable and they have optically smooth meniscus surfaces. Light can be modulated by simple adjustment of the flow conditions, thus eliminating the need for mechanical or electrical parts for manipulating the lens on the microchip.

Optofluidic lenses can be categorized into in-plane and out-of-plane lenses, depending on the light propagation direction (Song & Tan, 2017; Nguyen, 2010). Yu et al. presented a hydrodynamic out-of-plane optofluidic lens consisting of two layers, which was fabricated by soft lithography, as shown in Fig. 10.5a (Yu et al., 2010). The lower layer contains a circular PDMS aspherical surface that can effectively compensate spherical aberration and improve optical quality, and the upper layer is a PDMS elastic membrane. By controlling injection pressure in the microchannel, the surface contour of the upper layer can be changed, and the focal length of the lens is dynamically adjusted. Other approaches such as using stimuli-responsive hydrogels (Dong et al., 2006), electrical tuning (Mishra et al., 2014), and changing medium's refractive index (Hu et al., 2018) have also been exploited to adjust the focal length of out-of-plane optofluidic lenses.

Since the fabrication process of out-of-plane lenses is relatively complex and the structures should be well-aligned, their applications in optofluidic systems are

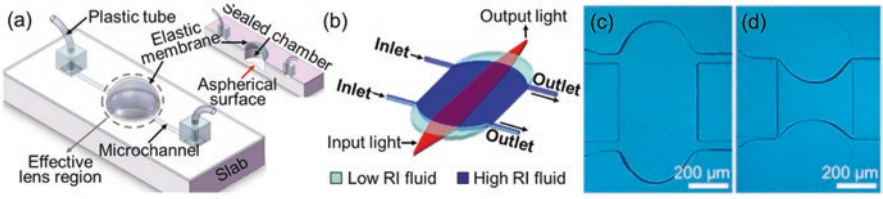

Fig. 10.5 (**a**) Schematic on a liquid-filled out-of-plane lens. The inset illustrates the cross section of the device. (**b**) Schematic on an in-plane optofluidic lens. The high RI fluid medium forms a biconvex microlens that focuses the incident light. (**c**, **d**) Experimental images on the biconvex microlens (**c**) and the biconcave microlens (**d**), respectively. (Reproduced with permission (Chen et al., 2019), Copyright 2019, Optical Society of America)

limited in many cases (Nguyen, 2010; Mao et al., 2009). In-plane optofluidic lenses, on the other hand, offer more compatibility. The geometry of in-plane optofluidic lens can be changed to adjust focal length by pneumatic tuning (Shi et al., 2010), thermal driving (Liu et al., 2017a), etc. Hydrodynamic tuning is well studied and widely used; this method is based on the formation of a curved liquid/liquid interface, which is controlled by hydrodynamic force. A curved fluid interface can be generated between a core stream and a cladding stream, and this feature can be used as an optofluidic lens and altered by simply changing the flow rate. Mao et al. firstly reported an on-chip hydrodynamically tunable liquid-liquid microlens (Mao et al., 2007). Later, Rosenauer et al. designed a hydrodynamically adjustable convex lens with 3D light focusing ability (Rosenauer & Vellekoop, 2009b). Two miscible fluids of different refractive indices were co-injected into a 90-degree curve in a microfluidic channel. Upon entering the curve, a centrifugal effect caused the fluidic interface to be distorted and one liquid bowed outward into the other. The bowed fluidic interface, coupled with the refractive index contrast between the two fluids, generated the microlens. The curvature of the fluidic interface was modulated by changing the flow rate. Higher flow rates generated a microlens with larger curvature and hence shorter focal length. Hydrodynamically tunable lenses can also be formed in microfluidic channels, in which part of the channel sections are expanded. Fang et al. also presented a hydrodynamic optofluidic lens (Fang et al., 2017). Silicone oil and $CaCl_2$ solution can be injected into an expanded chamber, and used as cladding and core layers of the lens (Fig. 10.5b), respectively, wherein the refractive index of the cladding streams matches that of the device's material to avoid light scattering. By tuning flow rates, the lens geometry can be changed into biconvex (Fig. 10.5c), plano, or biconcave format (Fig. 10.5d). The incident light therefore can be converged, collimated, or diverged, respectively.

Interestingly, it has also been reported that biological materials such as cyanobacteria (Schuergers et al., 2016), diatoms (De Tommasi et al., 2014), red blood cells (RBC) (Miccio et al., 2015), and spider silks (Monks et al., 2016) also show the capability to focus light into a confined region, acting as bio-microlens. Miccio et al. demonstrated using RBC as adaptive optofluidic microlens to perform real-time, fine-resolution measurement on chip (Miccio et al., 2015). Li et al. trapped living yeast and human cell with spherical or disc shapes on a fiber probe to confine excitation light in a sub-wavelength region and achieve fluorescence enhancement (Li et al., 2017).

10.3.6 Integrated Optical Detector

Many optical detectors have been integrated on microfluidic chips, such as silicon photodiodes (Kamei et al., 2003), organic photodiodes (OPDs) (Hofmann et al., 2005), and complementary metal-oxide-semiconductor (CMOS) chips (Cui et al., 2008; Lee et al., 2007). The former two are point detectors without spatial resolution, whereas CMOS detectors can capture a whole image. Silicon photodiodes

could render relatively high-sensitivity detection of low analyte concentrations but are too expensive and complicated to fabricate as an integral part of a disposable microfluidic chip. Generally speaking, the optical detectors integrated in point-of-care devices should be inexpensive and easy to fabricate. In contrast to the silicon counterpart, OPDs represent a promising option, as the substrates for their microfabrication can be either a glass or a polymer instead of silicon. For example, when the OPD substrate was printed on a glass slide (Wojciechowski et al., 2009), this system approached the final requirements of a point-of-care system, i.e., it was inexpensive, easy to use, highly sensitive, and robust. Besides realization of photodiodes, CMOS technology allows another type of detector that can be assembled on microfluidic chips and offers the great advantage of the ability to observe the image of the sample object. One of the most widely developed applications of an integrated CMOS detector on-chip is lens-free imaging (Greenbaum et al., 2012). Typically, bio-imaging and biosensing are performed at the microscopic scale, and this usually requires lenses integrated in a microscope system. Lens-free imaging has matured as a modality competitive with traditional lens-based microscopy. In lens-free microscopy, a diffraction pattern resulting from an object is recorded directly on a digital image sensor array without being optically imaged or magnified by any lens elements (Ozcan & McLeod, 2016). Compared to conventional microscopy, this technique is portable and cost-effective, and it provides a field of view of the same size as the sensor size and a numerical aperture close to 1, since the large-area detector is placed very close to the sample. This architecture is advantageous to make the microfluidic system as compact as possible and provides high photon collection efficiency in fluorescence microscopy. Therefore, it is suitable for analysis applications requiring large statistics, such as cytometry. Ozcan's research group has developed different lens-free holographic imaging platforms for on-chip cytometry and diagnostics, with either fluorescent imaging format (Zhu et al., 2011; Arpali et al., 2012) or shadow imaging format (Seo et al., 2009; Wei et al., 2013). Zhu et al. demonstrated a compact optofluidic platform that integrated imaging cytometry and fluorescent microscopy and could be attached to a cell phone (Zhu et al., 2011). The resulting device could be used to rapidly image bodily fluids for cell counts or cell analysis. However, fluorescent labels are unsuitable for a high-resolution lens-free holographic imaging setup because their emission is incoherent with their excitation. Instead, beads with biomolecularly functionalized surfaces can be used to provide specificity, as the scattering from these beads is coherent with their illumination (Ozcan & McLeod, 2016). Wei et al. proposed using gold and silver nanobeads as specific labels to identify and count the number of CD4 and CD8 cells in a cell suspension (Wei et al., 2013). CD4 and CD8 cells are specific types of T lymphocytes, and their relative populations are important for evaluating the stage of human immunodeficiency virus (HIV) infection or AIDS, as well as for evaluating the efficacy of antiretroviral treatment. Counting the relative populations of these cells can be challenging, however, because the only significant difference between these cells is in the types of proteins expressed on their membranes. Under a microscope, both types of cells look virtually identical. In order to sense and count these cells in a lens-free imaging setup, the authors used gold nanoparticles functionalized with

anti-CD4 antibodies to label CD4 cells and silver nanoparticles functionalized with anti-CD8 to label CD8 cells. By comparing the spectral response of different cells under lens-free imaging, the investigators were able to discriminate these two types of cells with greater than 95% accuracy using a machine learning algorithm.

To summarize, optofluidic components have shown great potential with respect to various on-chip optical process. It is envisioned that all optical components can be integrated into a single chip in the near future, as well as full functionalities. In terms of highly sensitive bioanalytical analysis in an integrated platform, such optofluidic components and their combinations have to address several critical challenges. Firstly, unlike solid-state optical elements, physical properties of a liquid medium are prone to be instable and temperature dependent, and any disturbance such as heat dissipation would compromise device's performance. Flow control is another concern whenever continuous liquid supply is required. Especially, most structural materials in microfluidic systems have refractive indices very close to the refractive index range of liquids, which hamper the capability to tightly focus a light beam with high numerical aperture. These challenges therefore need more research efforts to develop new approaches.

10.4 Fabrication Technologies of Optofluidic Components

Fabrication of micro-optical devices mainly relied on techniques transferred from the conventional two-dimensional (2D) integrated circuit (IC) and two- or three-dimensional (3D) MEMS processes. Semiconductor fabrication techniques have been adopted to micro-optical structures, including photolithography, thin-film deposition, chemical etching, etc. Silicon-, glass-, glass-silicon-, and glass-polymer-based fabrication techniques were widely studied. However, silicon and glass are hampered from wider applications in micro-optics, because they possess micromachining difficulties and are relatively expensive; moreover, an inconvenience of silicon is the lack of optical transparency at ultraviolet (UV), visible, and near-infrared (IR) wavelengths. Tremendous effort has been made to find alternative materials that are more cost-effective and easier machinable. With the development of related fabrication techniques, polymer−/plastic-based devices have therefore gained increasing interest. Compared with silicon and glasses, polymer materials can avoid high-temperature annealing and stringent cleaning (if they are disposable), and they are more cost-effective and have easier microfabrication, and there exists a wider range of materials to be chosen for characteristics that are required for each specific application, such as good optical transparency, biocompatibility, and chemical or mechanical properties. However, polymer materials usually do not result in strongly bonded layers like glass or silicon, and can exhibit structural deformation during device packaging processes. Each material has therefore both its advantages and disadvantages, and the choice of it will depend on the specific application. New technologies have also been developed in the meanwhile. This section presents current fabrication methodologies to make microfluidic and micro-optic structures.

10.4.1 Microfluidics Technologies

Current methods for fabrication of microfluidic devices can be categorized as replication techniques, such as soft lithography, and direct subtractive fabrication techniques such as laser micromachining (Wu & Gu, 2011).

Soft lithography typically refers to the molding of PDMS, using master templates. PDMS is inexpensive, is biocompatible, and has excellent liquid sealing properties, making it very suitable for microfluidics. In addition, it can be easily bonded to itself, allowing the fabrication of multilayer structures. Thin PDMS diaphragms are elastically extensible so that much larger deflections can be achieved than with hard materials. Fabrication of PDMS structures with micromolding is normally accomplished with four steps: first, a mold (i.e., the master) is fabricated (see Fig. 10.6a) (Duffy et al., 1998). This mold is usually fabricated in photoresist, such as SU-8, by photolithography, or it can also be made by silicon or metal suing chemical etching or laser micromachining techniques. Depending on the mold material and topography, a surface treatment is usually recommended in order to facilitate de-molding. Subsequently, a prepolymer solution (a mixture of PDMS linear polymer and a cross-linking agent) is poured on top of the mold. For high-aspect-ratio mold topographies, this step may need to be performed under vacuum to remove air bubbles. Then, the polymerization is completed. This procedure can be performed for 1–24 h, depending on the curing temperature. Lastly, the PDMS layer is carefully peeled off from the master and then bonded to a substrate material to form a full device. The mold can be reused many times, which reduces the cost considerably. Overall, soft lithography is faster, less expensive, and particularly suitable for prototyping compared to glass and silicon micromachining. Therefore, this method is commonly used for fabricating various microfluidic devices.

Other than soft lithography, *hot embossing* and *injection molding* are widely used to mold plastic materials. *Hot embossing* is a technique that transfers a pattern from a micromachined silicon, quartz, or metal master to a pliable plastic sheet (see Fig. 10.6b) (Li, 2015a). Heat and high pressure allow the plastic sheet to become imprinted. First, the stamp or master is brought in contact with the plastic surface. A well-distributed pressure is applied, while the substrate is heated to above its glass transition temperature. Finally, the substrate is cooled down before removing the stamp. *Injection molding* is another very promising technique for low-cost fabrication of microfluidic devices (see Fig. 10.6c) (Li, 2015b). Thermoplastic polymer materials are heated past their glass transition temperature to make them soft and pliable. The molten plastic is subsequently injected into a cavity that contains the master. Because the cavity is maintained at a lower temperature than the plastic, rapid cooling of the plastic occurs, and the molded part is ready in only a few minutes.

Even though polymer materials are now widely used in microfluidic devices, they still have drawbacks such as poor electrical and mechanical properties, and less resistance to many common solvents. In optofluidics, damage upon tightly focused laser irradiation and fluorescence at certain common wavelengths appear to be

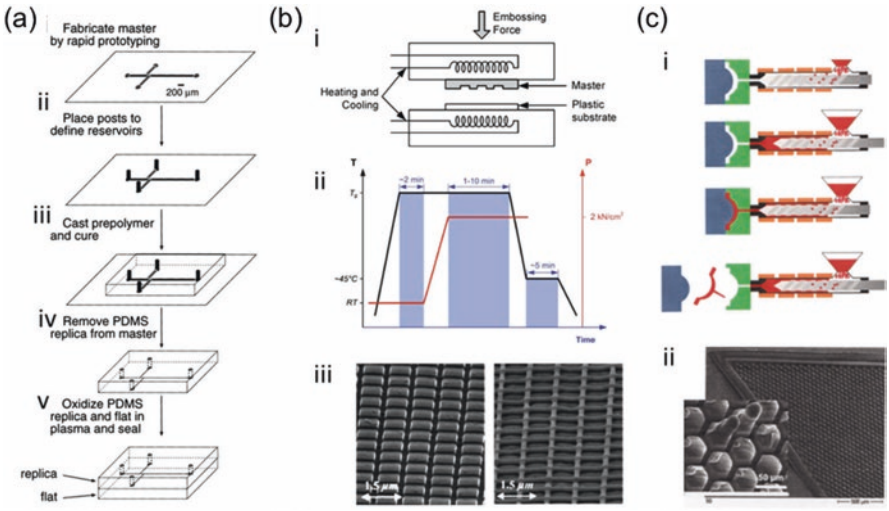

Fig. 10.6 (**a**) Scheme describing the fabrication of enclosed microscopic channels in PDMS. (i) A photoresist master is realized on a silicon wafer. (ii) Glass posts were placed on the wafer to define reservoirs for analytes and buffers. (iii) A prepolymer of PDMS was then cast onto the silicon wafer and cured. (iv) The polymer replica of the master containing a negative relief of channels was peeled away from the silicon wafer, and the glass posts were removed. (v) The PDMS replica and a flat slab of PDMS were oxidized in a plasma discharge and were brought into conformal contact, so that an irreversible seal formed between them. (**b**) (i) Schematic diagram of a hot embossing tool. (ii) Typical temperature (T) and pressure (P) conditions during a hot embossing process. (iii) Silicon master and the embossed PMMA structure. Features are 150 nm wide and 200 nm deep at 1 µm spacing. (**c**) (i) Schematic diagram of an injection molding process. (ii) Injection-molded polymer structures. (Reproduced with permission (Yang & Gijs, 2018), Copyright 2018, Royal Society of Chemistry)

severe when using polymer materials. In contrast, glass-based devices with high optical transparency to visible light and inertia to chemical solvents prove to be very suitable for these applications. Therefore, glass has still been widely used in the commercial biosensing products. Companies such as Micronit, LioniX, or Micralyne market glass microfluidic circuits.

Typical fabrication technique on glass substrate is laser micromachining. *Laser micromachining* is a direct write and etch technique; therefore, it does not require any mask or post-development steps. It is a suitable technique for rapid prototyping of microsystems, and in particular microfluidic devices. Most glasses have poor thermal properties and are brittle, which makes the fabrication of finely machined features a difficult task. In this regard, ultrafast laser microfabrication, which utilizes ultrashort laser pulses of pulse width as narrow as ~100 fs (a femtosecond laser), became a powerful approach for precise and fine processing for optofluidic devices in glasses (Zhang et al., 2008). By exposing a piece of glass to a focused femtosecond laser of a peak intensity well above the damage threshold of the glass, three-dimensional microstructures could be generated in the glass. A unique feature of laser micromachining using a femtosecond laser is that it can deliver high-density

energy in a highly controlled and spatially localized way. The nonlinear absorption induced by the extremely high peak intensity in the pulse's focal point ensures that the absorption, and therefore material removal, is confined to the vicinity of the focus, leaving the rest of the substrate unaffected, thus allowing ultraprecision micromachining. In addition to the fabrication of microchannels in glass, microchannels can also be fabricated in polymers by femtosecond lasers (Zheng et al., 2006; Gattass & Mazur, 2008). By direct writing on a glass substrate, a femtosecond laser beam with a small pulse energy (< micro-Joules) can generate a localized increase on the refractive index in the material, therefore generating a waveguide. Moreover, if the peak intensity of the laser pulse is higher than the damage threshold of the glass, the material at the focus is vaporized, and the high pressure pushes the material to both sides of the irradiated region. Consequently, the tracks at the two sides result in a higher refractive index, while the region between the two tracks can guide light. Compared with MEMS techniques, laser microfabrication offers the advantages of simplicity, versatility, and high efficiency. Because there is no need for either a mask or post-development processing, the fabrication rate using femtosecond lasers is approaching that of lithographic techniques, though a femtosecond laser remains a very expensive equipment.

10.4.2 Micro-Optics Technologies

Micro-optical and optofluidic devices have also benefited from microelectronic technology development. This section reviews current fabrication methodologies to make optical structures on a chip, focusing on integrated waveguides and microlenses.

10.4.2.1 Technologies for Waveguide Fabrication

On-chip integrated waveguides can be easily interfaced with external light sources and detectors, while they precisely direct light to the microfluidic channel, both for providing the optical source to locally expose the targets and precisely directing the scattered or fluorescent output signals to the external detectors, without the difficulties of alignment, epoxy-fixing, or breakage problems, occurring when using fibers. Therefore, waveguides have been widely used in integrated microsystems. Integrated waveguides can be constructed using a variety of micromachining procedures. Common processes include lithographic patterning, thin-film deposition, and etching, and these techniques can be used to fabricate a ridged waveguide, i.e., a solid-core waveguide. Usually, a thin layer of the core material is deposited on a planar substrate first. The substrate is coated with photoresist, the latter is then exposed to UV light or X-rays through a lithography mask that defines the waveguide shape, and developed to form a pattern on the surface of the substrate. With the remaining photoresist as a mask for either wet chemical or dry etching to define the ridge

waveguide structures. Dry etching methods, for example ion-beam etching, produce smooth edges, particularly on curved sections, but they also cause some lattice damage, which must be removed by annealing if minimum optical losses are desired. Wet chemical etching on the other hand produces less lattice damage, but it is very difficult to control the etch depth and profile. Most chemical etchants are preferential regarding crystal orientation, thus leading to ragged edges on curved sections of waveguides when using Si substrates. After the photolithography and etching procedures to process the core, a cladding layer is deposited. As an example, silicon oxynitride waveguides were fabricated in a standard silicon fabrication line by PECVD and LPCVD deposition processes in combination with 1100 °C annealing treatments to remove light-absorbing hydrogen bonds, and optical lithography for pattern definition and dry RIE for the pattern transfer process (Aparicio et al., 2014). As shown in Fig. 10.7, a 2-μm-thick SiO_2 buffer layer (n = 1.45) and a 1-μm-thick SiO_xN_y core layer (n = 1.85) were both deposited by PECVD; a ~0.5-μm-thick borophosphosilicate glass (BPSG) layer (n = 1.45 nm) was grown by LPCVD in order to optimize the surface planarity after RIE. Finally, the whole system was coated with a thin SiN_x film (50 nm of thickness). This waveguide system was applied to detect low surface concentration (10^{-11} mol cm^{-2}) of a green light-emitting organic dye.

While a solid-core waveguide is assembled into the microchip but fabricated separately from the microchannels, liquid-core waveguides (LCWs) share the same physical volume as the microfluidic channels. Indeed, the microchannel not only transports the sample but also transmits the light, which greatly simplifies the design and reduces light loss through the channel walls. There are many different methods to fabricate LCWs. By using the soft lithography technology to mold PDMS structures, Cho et al. developed a method to construct LCWs in PDMS microchannels by

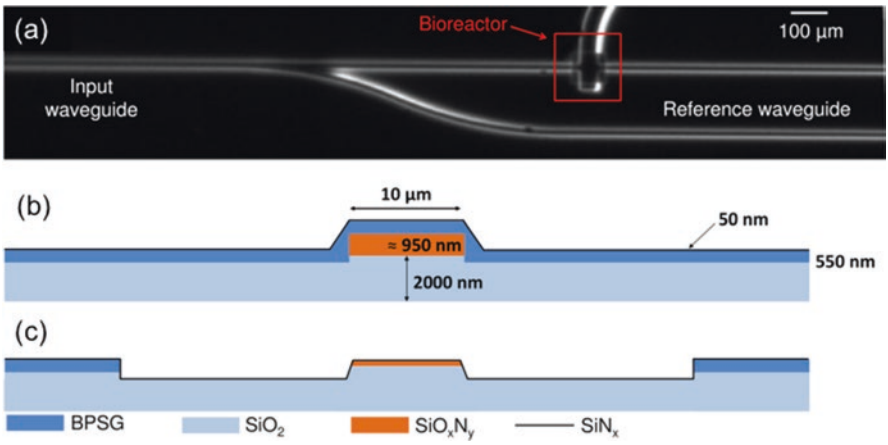

Fig. 10.7 Fabrication procedure of silicon oxynitride waveguides: (**a**) Optical image of the top view of the waveguide; (**b**, **c**) Schematic cross sections of the waveguide structure before (**b**) and at the bioreactor well (**c**). (Reproduced with permission (Yang et al., 2019), Copyright 2019, MDPI)

flowing Teflon® AF solution through the channels (Cho et al., 2010a). This coating approach avoids the difficulty of bonding between two Teflon-coated substrates. The waveguide was integrated into a micro fluorescence-activated cell sorter that, by readout of the fluorescence signal of pre-stained cells, could sort the latter into a split channel positioned downstream.

10.4.2.2 Technologies for Microlens Fabrication

A microlens is an important key component for focusing and collimating light. It can be made as a solid curved surface or as a tunable interface between two deformable materials/media. On-chip hard solid-state lenses usually are fixed-focus lenses, similar to miniaturized traditional lenses that are used in a free-space detection system. Different methods have been developed for building solid microlenses. Thermal reflow processes have been widely used for the fabrication of large arrays of hemispherical microlenses. In this technique, a glass substrate is first coated with a layer of photoresist. Photolithography technique is then used to pattern the photoresist layer and generate a series of cylindrical islands, which are heated above the glass transition temperature of the photoresist. Due to surface tension, the shape of the photoresist cylinders changes to minimize the surface energy and becomes hemispherical, therefore generating a microlens array on the substrate. As the surface tension governs the contact angle of the photoresist and the shape of the microlens eventually, a thin layer of additives can be deposited on the substrate to influence the surface tension between the substrate and the photoresist, tuning the focal length and numerical aperture of the fabricated lenses. Yang et al. utilized a bottom polyimide layer to form a pedestal to sustain the upper photoresist lens after the heat reflow process (Yang et al., 2004). The interactive force between two material interfaces causes the upper photoresist to form a spherical profile and transform the polyimide pedestal into a trapezoid with arc sides (as shown in Fig. 10.8). Advantages of the thermal reflow technique include a low material consumption, low manufacturing costs, the intrinsic simplicity of the technique, and an easy process control. Microlens arrays can be produced over large surface areas. However, the low transparency and thermal instability of photoresist features during the reflow process limit its widespread application (Yang & Gijs, 2018).

Tunable microlenses are based on adjusting the curvature of the interface between two media, such as liquid/liquid, liquid/air, and liquid/soft solid interfaces. These microlenses are dynamic optical elements, and their focal length can be tuned by changing either the refractive index or the geometry of the microlens. The refractive index of the liquid in a micro-optofluidic device can be modulated by changing fluid characteristics, such as species, concentration, and flow patterns of liquid streams. The geometry of the lens can be modulated by a variety of concepts known in microfluidics. If the lens is formed by a liquid/solid interface of a soft material such as PDMS, the shape of a thin flexible membrane spanning a cavity with the fluid inside can be controlled by applying pressure. If the lens is formed by liquid/liquid or liquid/air interfaces, its shape can be controlled by means of hydrodynamics,

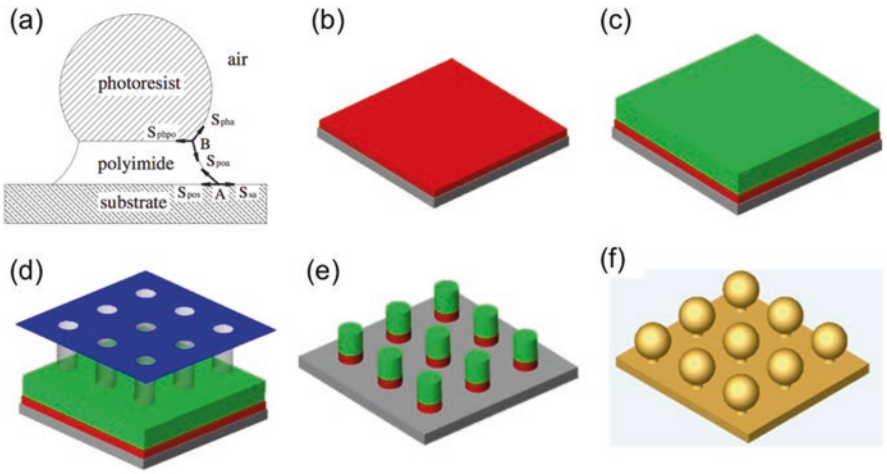

Fig. 10.8 Illustration of a micro-ball lens formation in the thermal reflow process. A polyimide layer is coated on a Si wafer beneath a photoresist layer. Photolithography process is used to pattern these two materials through a mask. Micro-ball lens array with a pedestal can be generated after heat reflow. (Reproduced with permission (Yang et al., 2019), Copyright 2019, MDPI)

electro-wetting, or other physical effects. When the lenses are tuned by manipulating the refractive index of a liquid, the composition of the lens liquid can be changed by controlled diffusion of species. With microfluidic techniques, when a laminar flow condition is maintained in the microfluidic channel, the concentration distribution of species is determined by molecular diffusion. Thus, a concentration gradient or a refractive index gradient can be generated along the flow direction. Mao et al. reported a liquid gradient refractive index (L-GRIN) lens (Mao et al., 2009). The lens was formed by diffusion of $CaCl_2$ from a core stream with a concentration of 3.5 M to cladding streams of deionized water (see Fig. 10.9). The refractive index decreased gradually from $n = 1.41$ to $n = 1.33$. The concentration profile and the corresponding refractive index profile could be controlled by the flow rate of the core stream and the two cladding streams. By adjusting the flow rates, a large gradient of refractive index was achieved, and it allowed a sharper bend of light beams, resulting in a shorter focal length. By adjusting the flow rate of the cladding streams asymmetrically, the concentration profile swung to one side, allowing the light beam to be focused off the optical axis.

10.5 Optofluidic Devices for Bioanalytical Application

This section introduces the main applications of optofluidic systems, and we will focus on cytometry and cell biology studies, as well as nucleic acid and protein detection systems.

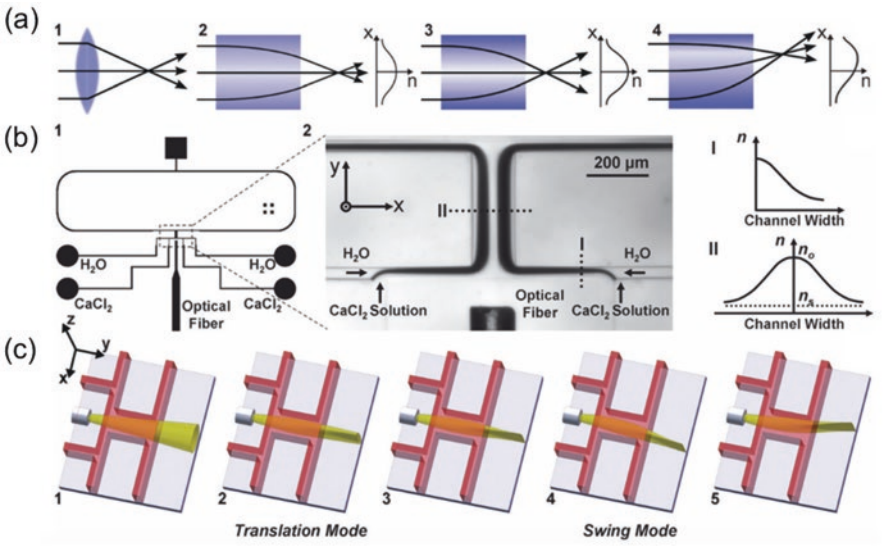

Fig. 10.9 Principle and design of a liquid gradient refractive index (L-GRIN) lens. (**a**) A schematic diagram showing the comparison between the classic refractive lens (a1) and GRIN lens (a2). Change of the refractive index contrast in GRIN lens can result in change of focal distance (a2–a3), and shift of optical axis can result in change of output light direction (a4). (**b**) Schematic of the L-GRIN lens design (b1), microscopic image of the L-GRIN lens in operation (b2, left), and the expected refractive index distribution at two locations (I and II) inside the lens (b2, right). High optical contrast areas (dark streaks) were observed near the fluidic boundaries (b2, left), suggesting significant variation of refractive index due to the $CaCl_2$ diffusion. (**c**) Schematic drawing showing two operation modes of the L-GRIN lens: the translation mode with variable focal length including no-focusing (c1), a large focal distance (c2), and a small focal distance (c3); and the swing mode with variable output light direction (c3–c5). Illustration of a micro-ball lens formation in the thermal reflow process. A polyimide layer is coated on a Si wafer beneath a photoresist layer. Photolithography process is used to pattern these two materials through a mask. Micro-ball lens array with a pedestal can be generated after heat reflow. (Reproduced with permission (Yang & Gijs, 2018), Copyright 2018, Royal Society of Chemistry)

10.5.1 Cytometry and Cell Biology Studies

Flow cytometry or fluorescence-activated cell sorting (FACS) is a commonly used powerful analytical technique in research, in which the properties of individual elements of a population, such as cells or microparticles, are measured. It has a wide range of applications, including immunophenotyping, gene diagnosis, bacteria analysis, and clinical hematology diagnosis. Typically, these applications require the labeling of cells with multiple fluorophores for correlated analysis of cellular characteristics and properties. Fluorescently tagged antibodies are often used to mark and identify cells via immunofluorescence (Godin et al., 2008). After the labeling procedure, the cells are introduced in a fluidic system and hydrodynamically focused by a sheath flow, ensuring that cells travel through the center of the

fluidic channel at a uniform velocity. The cells pass an optical interrogation zone one by one, where they are illuminated by a light source. The light beam normally passes perpendicularly across the microfluidic channel. As each cell is illuminated, it scatters light with a characteristic directional intensity distribution. An optical detection system, which consists of waveguides/optical fibers, lenses, photodetectors, etc., guides and collects the detection signals. Thus, the light scattered from the cell and one or more colors of fluorescence emitted from the illuminated cell are measured, providing a number of parameters to yield statistics about the sample subpopulations. After identification by the optical system, a downstream sorting system can isolate cells of interest (Piyasena & Graves, 2014).

There has been extensive work on miniaturizing benchtop flow cytometers into microfluidic systems; the advantage of the latter is that they can operate with small sample (and thus reagent) volumes, lowering the cost of assays and experimentation. Moreover, a highly integrated chip-based approach would turn much of the time-consuming and expensive work of setup optimization and troubleshooting into simple chip replacement. This should significantly reduce or eliminate the need for costly service contracts and dedicated maintenance personnel (Cho et al., 2010b). Following the practice of commercial instruments, many microfluidic cytometers still use traditional bulk optics and typically require a confocal microscope stage for mounting commercial high-magnification objectives. However, when the optical components can be co-integrated onto a single chip, the probability of hardware failure will be reduced. More importantly, an optofluidic cytometer offers the potential for innovative architectures and increased functionality. The high-level integration, along with parallel processing techniques, can be exploited for screening at higher throughput. Many different formats of waveguides and microlenses have been integrated on-chip for improving the optical system performance. For example, Watts et al. presented a functional photonic-microfluidic flow cytometer with integrated optical waveguides and beam shaping components (Watts et al., 2010, 2013). The waveguide cores, optical lenses, and microfluidic channels were simultaneously fabricated in SU-8 on a glass substrate, which also served as a bottom cladding region. PDMS was used to seal the fluid channels and to simultaneously act as the upper cladding of the waveguides. Air regions formed by removing material from either side of a waveguide core region formed the side cladding of the waveguides. The ridge waveguide terminated at a system of vertical cylindrical lenses that were designed to focus the input beam originating from the waveguide into a tunable spot in the middle of the microfluidic channel. Beam waists of different width could be obtained via changing the lens design to detect particles with different sizes (Watts et al., 2010). In order to enhance the detection of the forward scattered light in the microfluidic flow cytometer, a notch was placed in the lens system, which caused a dark spot on the facet of a collection waveguide. This design helped to remove axial rays from the excitation beam and decreased the background noise (Watts et al., 2013).

Other than cytometric analysis, optofluidic systems have also been used for manipulation of cells and for cell biology analysis. The application of optofluidic technologies for various optics-based single-cell analyses, which involved

single-cell manipulation, treatment, and physical property detection, was reviewed by Huang et al. (2014). Optical tweezer-based single-cell manipulation is based on the generation of a large electromagnetic field gradient at the focal point of a beam of light formed by a lens. This resulted in an attractive force that pulls the particle to the focused spot, if the particle permittivity is larger than that of the surrounding medium. Another strategy adopted to optically manipulate cells is the use of scattering forces induced by a laser beam to push cells to certain areas on the chip. Moreover, researchers have demonstrated the use of optically induced mechanical and electrical forces to perform single-cell manipulation. For example, a high-power laser pulse generated a microbubble that provided the actuation force to transport a cell to a collection channel (Chen et al., 2013). Micro-optical structures not only have been used for generating forces for on-chip cell manipulation, but also were at the basis of biophysical characterization of cells and cellular phenotyping in general. An overview of the different optical detection methods that have been used for the latter was presented in the review article of Tung et al. (2012). Herein, optofluidic devices were categorized according to the different detection techniques used, namely, fluorescence, surface-enhanced Raman spectroscopy, surface plasmon resonance, or interferometric detection. Rodriguez-Ruiz et al. have discussed the engineering aspects of integrating optical spectroscopy with microfluidic systems, such as making the choice of the appropriate detection mechanism, i.e., colorimetry, fluorimetry, absorbance, and/or dispersion/scattering to be combined with microlenses of different materials and mirrors, depending on the application (Rodríguez-Ruiz et al., 2016).

Ibarlucea et al. demonstrated cell screening in a disposable PDMS chip operating in a multiple internal reflection detection mode configuration (Ibarlucea et al., 2010; Vila-Planas et al., 2011). The chip was tailored such that the interrogation region of the sample allowed reducing the mean flow cell volume by including self-aligned lenses and focusing mirrors on the chip. In particular, light propagating in the system followed a zigzag optical path with the help of integrated air mirrors (see Fig. 10.10a). The system was able to perform either scattering, scattering + absorption, or absorption measurements without any hardware modification. Later the same group demonstrated a monolithically integrated biophotonic lab-on-a-chip for cell culture and simultaneous pH monitoring (Muñoz-Berbel et al., 2013). The device incorporated a filter with 3-μm-high size-exclusion microchannels, capable of efficiently trapping cells in the incubation chamber, as well as optical elements for real-time interrogation of two microfluidic chambers. Both yeast cells and vascular smooth muscle cells as a mammalian cell model were tested. Liang et al. measured the refractive index of single living cells transiting in a microfluidic channel (Liang et al., 2007). Chemical or ingredient changes inside a cell can be detected by its refractive index measurement; one of the possible applications is to distinguish cancer cells from healthy cells. The measurement system integrated an external cavity laser (the microfluidic channel with/without passing cell was part of the optical cavity) and a microlens (see Fig. 10.10b). When a cell was transiting through the cavity, this resulted in a frequency shift and intensity modulation of the power of a broadband laser source, from which one derived the cell's refractive index.

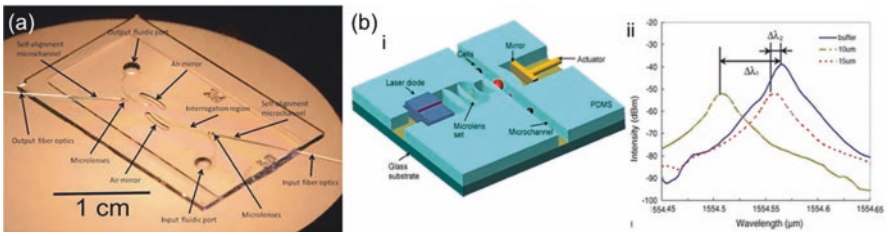

Fig. 10.10 (**a**) Picture of a PDMS-based multiple internal reflection system. It comprises self-alignment microchannels for accurate fiber optics positioning, microlenses, and air mirrors. All these micro-optical elements ensure an adequate zigzag path of the light along the interrogation region, which can be filled through the input fluidic port. (**b**) (i) Schematic diagram of an integrated optical cavity detection chip. Cells or microparticles are delivered into the external cavity of a laser along a microfluidic channel with a width of 100 μm. On account of the different indices between a living cell and the buffer medium, the cell moving through the analysis region changes the effective length of the external cavity and subsequently affects the emission characteristics of the laser diode. (ii) Experimental results for detection of PS beads, showing the emission spectrum obtained for the loaded PBS buffer, a 10 μm bead, and a 15 μm bead, respectively. (Reproduced with permission (Yang & Gijs, 2018), Copyright 2018, Royal Society of Chemistry)

Calibration of the system was based on the use of two standard PS beads of known refractive index. It was found that tested cancerous cells had a refractive index in the 1.392–1.401 range, while this was in the 1.35–1.37 range for normal cells.

10.5.2 Nucleic Acid and Protein Detection

There is a significant demand nowadays for high-throughput biomolecular analysis tools to assist diagnosis in research and clinical applications. Both DNA and proteins are frequently used to correlate biomarkers to specific diseases. Microfluidics offers quantifiable benefits over existing procedures in nucleic acid and protein analysis. PCR and fluorescence detection on microfluidic devices have led to a significant improvement in total processing time. While featuring low limits of detection, microfluidic devices can also improve the sensitivity and speed and reduce costs of an immunoassay over ELISA by overcoming the issues of the large sample and reagent volumes. Furthermore, by integrating different steps into a miniaturized system, microfluidics can also overcome the limitations of the use of multiple instruments with sample loss due to large dead volumes and the risk of contamination.

Detection schemes that rely on integrated optics have successfully demonstrated DNA fragment analysis. Both optical fibers and integrated waveguides have been used to deliver fluorescence excitation light into the system and collect emitted fluorescent signals. Guo et al. presented an optofluidic device to perform detection of DNA and its mutations (Guo et al., 2012). The device was composed of a droplet-generation unit, a mixing and reaction unit, and a fiber-based optical detection unit

with two fibers precisely positioned through fiber grooves, one for fluorescence excitation and the other connected to an off-chip photomultiplier tube (PMT) for signal collection (see Fig. 10.11a). By detecting the fluorescence signal changes of the target DNA/molecular beacon complex in single droplets, the device was able to distinguish molecular beacon, wild-type single-strain DNA BRCA1, single-mutation single-strain DNA, and control single-strain DNA in droplets with a detection throughput of 2000 droplets per second. Cai et al. reported a microdevice using hybrid optofluidic integration for detection and quantification of Ebola virus (Cai et al., 2015). In this work, sample preparation and target preconcentration were implemented on a PDMS-based microfluidic chip, and liquid-core optical waveguides on a silicon chip were used for single nucleic acid fluorescence detection. Magnetic microbeads functionalized with a synthetic oligonucleotide were used to capture the target nucleic acids; the bonded nucleic acids were then thermally released from the beads, re-suspended and fluorescently labeled, and sent to the optofluidic chip for detection. Brennan et al. presented an optofluidic platform, which had integrated microfluidic channels for fluidic delivery, a resonant mirror waveguide for optical detection, and surface chemistry for covalent immobilization of DNA probes (Brennan et al., 2008). The integrated device detected DNA binding in two configurations: (1) as an excitation platform for fluorescence measurements with Cy3-tagged target DNA and (2) as a refractive index platform, where changes in effective refractive index due to binding were monitored.

Besides detection of DNA hybridization, various designs that integrated optical waveguides and microlenses with microfluidics have been proposed to improve detection characteristics in immunoassays. Waveguide systems have realized noise rejection improvements by probing a region of interest of only hundreds of nanometers from the surface in heterogeneous assays using evanescent field excitation, preventing emission from unbound bulk material. The main advantage of this technique is to guide the light very close to the microfluidic channel, and then ensure an excellent coupling efficiency between the waveguide and the microfluidic channel. Kemmler et al. developed a point-of-care system to simultaneously measure c-reactive protein, interleukin-6, and procalcitonin (Kemmler et al., 2009). The system consisted of a planar waveguide fluorometer, a fluidic setup, and exploited sandwich bioassays. By microarray technology, one specific type of antibody for each parameter was spotted on the surface of the waveguide, and the detection was fluorescence-based and worked with specific labeled antibodies. The light was guided in the waveguide creating an evanescent wave close to the surface, which excited the surface-immobilized fluorophores very efficiently. The detection limit of CRP, IL-6, and PCT were 0.35, 0.08, and 1 ng/mL, respectively, with using a sample volume of ~120 μL. Liu et al. developed a planar waveguide-based array immunosensor, allowing measurements of up to 24 analytes simultaneously (Liu et al., 2017b). In this system, laser light was coupled into a planar optical waveguide via a beveled angle, forming eight individual TIR spots where excitation and detection were enabled (see Fig. 10.11b). A multichannel microfluidic chip was employed to isolate the parallel TIR lines physically so as to form eight independent flow channels on the same chip, avoiding the cross-reactivity of antibodies and supporting

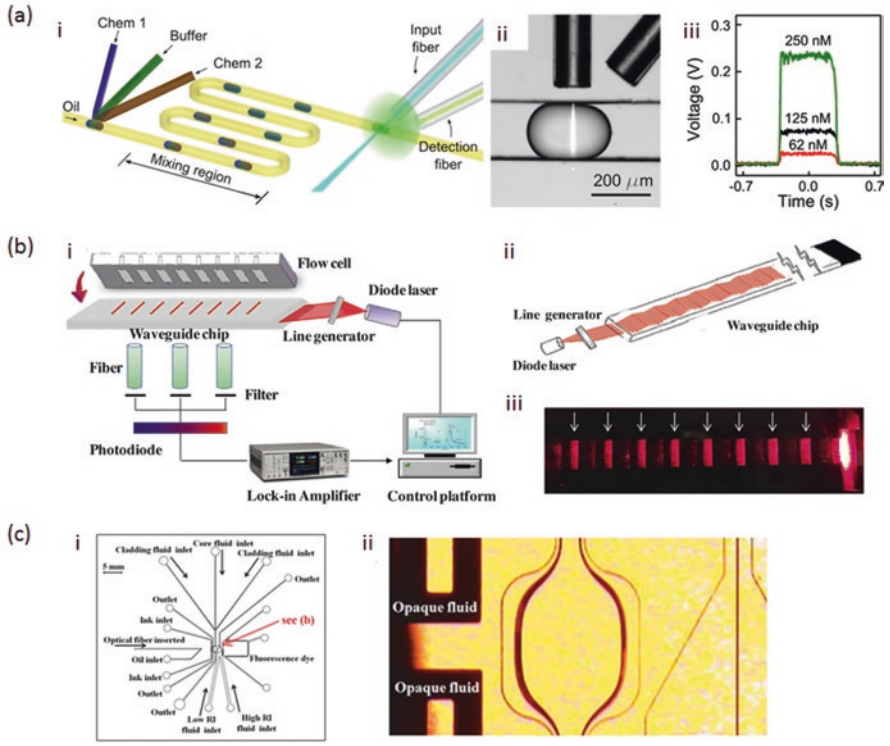

Fig. 10.11 (**a**) (i) Schematic of a droplet-based optofluidic device composed of a droplet-generation unit, a mixing and reaction unit, and a fiber-based optical detection unit. (ii) Fluorescence intensity characterization of the droplet-based with a microscopic snapshot of a droplet excited by a 20-μm-wide laser beam. (iii) Electric signal of three droplets with different fluorescent dye concentrations, as generated by a photomultiplier tube. (**b**) (i) Schematic diagram of a planar waveguide-based array immunosensor with a removable multichannel PDMS flow cell. (ii) Excitation light path inside the planar waveguide transducer. (iii) Photograph of waveguide chip with eight reflection lines for biosensing, as indicated by white arrows. (**c**) (i) Schematic illustration showing main components of a PDMS optofluidic chip comprising an all-liquid tunable in-plane biconvex microlens. (ii) Magnified image of aperture and microlens components of the optofluidic chip. (Reproduced with permission (Yang & Gijs, 2018), Copyright 2018, Royal Society of Chemistry)

various bioassay conditions. By employing fluorescent detection with fluorophore-labeled antibodies binding to the surface of the waveguide with the analyte derivative covalently attached, multi-analyte biosensing was realized.

Besides the aforementioned waveguides, also integrated microlenses have been used in optofluidic fluorescence systems to improve the system compactness and efficiency through more focused excitation of fluorescence volumes. Song et al. presented optofluidic lenses which were hydrodynamically formed with a liquid-core liquid-cladding configuration (Song et al., 2010, 2011). By tuning the flow rate ratio between core and cladding streams, the lens could be changed from focusing

mode into diverging mode, and the focal length and divergent angle were also tunable. The focusing effect of the converging lens was clearly observed by using the fluorescent dye rhodamine B. Chao et al. developed an optofluidic chip, which comprised a tunable in-plane biconvex microlens and micro-prism to control the focal length and deviation angle of a light beam (see Fig. 10.11c) (Chao et al., 2013). The L^2 microlens enabled the focal length to be adjusted in the range of 2.9–7.6 mm, while the microprism chamber filling with two fluids generated a deviation angle range of 6.2°–22.3°. Mohammed et al. demonstrated a capillary action-based autonomous microfluidic device in conjunction with on-chip planar microlenses, for optical detection of the cardiac biomarker troponin I (Mohammed & Desmulliez, 2013). The 2D planar lenses and the microfluidic channels were fabricated on a PMMA substrate using a single CO_2 laser process. The illumination from a single LED light source propagated through the microlenses and was focused onto an area of 0.5 mm^2, which represents the excitation area within the microfluidic channel, where a detection limit of 0.08 ng/mL was achieved, which is of the order of clinically acceptable concentrations. More related works are included in several review articles (Zhao et al., 2010; Threm et al., 2012; Schmidt & Hawkins, 2011).

10.6 Concluding Remarks

The integration of micro-optical elements with microfluidic platforms can advantageously contribute to the automation of many bioanalytical applications and that such miniaturized components are key to the improvement of the performance of an analytical system, especially when the latter has microfluidic features. Especially, the optofluidic integration results in high interaction efficiency between light and fluids, which is very desirable for sensing applications. In this chapter, optofluidic system for bioanalytical applications are exemplified, focusing on two main classes of components: optofluidic lasers and lenses. These elements have shown great potentials in various on-chip optical processes, but several challenges should be addressed such as disturbance on optical properties due to the instability of liquid medium, difficulty on flow control, and similar refractive indices between liquid and most structural materials of microfluidic systems.

In Sect. 10.2, we have concisely introduced basic features and advantages of engineered microfluidic systems that permit the implementation of all manipulation and handling steps necessary for designing an analytical process. We have then reviewed the field of micro-optics after introducing basic properties of electromagnetic waves and dielectric interface phenomena like scattering and refraction in Sect. 10.3. In Sect. 10.4, we have presented basic engineering building blocks of an optofluidic system, such as light sources, prisms, switches, optical detectors, and importantly micro-waveguides and microlenses. We presented also different technologies for realizing microfluidic and optofluidic chips in the next section. Current methods for fabrication of microfluidic devices and micro-optical components have been introduced. As main applications of microfluidic systems having on-board

integrated micro-optical components, we have consecutively discussed cytometric applications, cell biology studies, and nucleic acid and protein detection systems.

Summarizing, we believe that the integration of micro-optical components on a microfluidic chip presents key advantages for many large-scale biological studies at the individual cell level and is of benefit to automated analytical screening. We have shown that microfluidics and optofluidics have enormous potentials for replacing the traditional labor-intensive analytical procedures indeed. Moreover, these devices permit accurate spatiotemporal application of compounds, so that dose-response curves and screening data sets with enriched information can be obtained. Overall, optofluidic technologies largely demonstrated potential to dramatically improve many aspects of analytical research by providing superior performance when compared to the classical protocols. The ongoing transition of any modern analytical application from an observation-based discipline to a mechanism-based science suggests that systems capable of analyzing large samples in a well-defined spatiotemporal way and with better sensitivity will benefit from increasing attention in the next years and likely will become invaluable tools in the near future. Micro-optical components and optofluidic devices certainly will play a prominent role in this endeavor.

Acknowledgments This work was supported by the National Natural Science Foundation of China (61805271, 62074155), Key-Area Research and Development Program of Guangdong Province (2019B020226004), and Shenzhen Science and Technology Innovation Commission (JCYJ20170818154035069).

References

Aparicio, F. J., Froner, E., Rigo, E., Gandolfi, D., Scarpa, M., Han, B., Ghulinyan, M., Pucker, G., & Pavesi, L. (2014). Silicon oxynitride waveguides as evanescent-field-based fluorescent biosensors. *Journal of Physics D: Applied Physics, 47*, 405401.

Arpali, S. A., Arpali, C., Coskun, A. F., Chiang, H.-H., & Ozcan, A. (2012). High-throughput screening of large volumes of whole blood using structured illumination and fluorescent on-chip imaging. *Lab on a Chip, 12*, 4968–4971.

Brennan, D., Lambkin, P., Moore, E. J., & Galvin, P. (2008). An integrated optofluidic platform for DNA hybridization and detection. *IEEE Sensors Journal, 8*, 536–542.

Brown, M., Vestad, T., Oakey, J., & Marr, D. W. M. (2006). Optical waveguides via viscosity-mismatched microfluidic flows. *Applied Physics Letters, 88*, 134109.

Bruls, D. M., Evers, T. H., Kahlman, J. A. H., Lankvelt, P. J. W. V., Ovsyanko, M., Pelssers, E. G. M., Schleipen, J. J. H. B., Theije, F. K. D., Verschuren, C. A., Wijk, T. V. D., Zon, J. B. A. V., Dittmer, W. U., Immink, A. H. J., Nieuwenhuis, J. H., & Prins, M. W. J. (2009). Rapid integrated biosensor for multiplexed immunoassays based on actuated magnetic nanoparticles. *Lab on a Chip, 9*, 3504–3510.

Cai, H., Parks, J. W., Wall, T. A., Stott, M. A., Stambaugh, A., Alfson, K., Griffiths, A., Mathies, R. A., Carrion, R., Patterson, J. L., Hawkins, A. R., & Schmidt, H. (2015). Optofluidic analysis system for amplification-free, direct detection of Ebola infection. *Scientific Reports, 5*, 14494.

Campbell, K., Groisman, A., Levy, U., Pang, L., Mookherjea, S., Psaltis, D., & Fainman, Y. (2004). A microfluidic 2 × 2 optical switch. *Applied Physics Letters, 85*, 6119–6121.

Carney, P. S., & Schotland, J. C. (2001). Three-dimensional total internal reflection microscopy. *Optics Letters, 26*, 1072–1074.

Chao, K.-S., Lin, M.-S., & Yang, R.-J. (2013). An in-plane optofluidic microchip for focal point control. *Lab on a Chip, 13*, 3886–3892.

Chen, Z., Taflove, A., & Backman, V. (2004). Photonic nanojet enhancement of backscattering of light by nanoparticles: A potential novel visible-light ultramicroscopy technique. *Optics Express, 12*, 1214–1220.

Chen, Y., Wu, T.-H., Kung, Y.-C., Teitell, M. A., & Chiou, P.-Y. (2013). 3D pulsed laser-triggered high-speed microfluidic fluorescence-activated cell sorter. *Analyst, 138*, 7308–7315.

Chen, S., Hao, R., Zhang, Y., & Yang, H. (2019). Optofluidics in bio-imaging applications. *Photonics Research, 7*, 532–542.

Cho, S. H., Chen, C. H., Tsai, F. S., Godin, J. M., & Lo, Y.-H. (2010a). Human mammalian cell sorting using a highly integrated micro-fabricated fluorescence-activated cell sorter (μFACS). *Lab on a Chip, 10*, 1567–1573.

Cho, S. H., Godin, J. M., Chen, C.-H., Qiao, W., Lee, H., & Lo, Y.-H. (2010b). Recent advancements in optofluidic flow cytometer. *Biomicrofluidics, 4*, 043001.

Cui, X., Lee, L. M., Heng, X., Zhong, W., Sternberg, P. W., Psaltis, D., & Yang, C. (2008). Lensless high-resolution on-chip optofluidic microscopes for Caenorhabditis elegans and cell imaging. *Proceedings of the National Academy of Sciences of the United States of America, 105*, 10670–10675.

Darafsheh, A., Walsh, G. F., Negro, L. D., & Astratov, V. N. (2012). Optical super-resolution by high-index liquid-immersed microspheres. *Applied Physics Letters, 101*, 141128.

De Tommasi, E., De Luca, A. C., Lavanga, L., Dardano, P., De Stefano, M., De Stefano, L., Langella, C., Rendina, I., Dholakia, K., & Mazilu, M. (2014). Biologically enabled sub-diffractive focusing. *Optics Express, 22*, 27214–27227.

Dittmer, W. U., Evers, T. H., Hardeman, W. M., Huijnen, W., Kamps, R., Kievit, P. D., Neijzen, J. H. M., Nieuwenhuis, J. H., Sijbers, M. J. J., Dekkers, D. W. C., Hefti, M. H., & Martens, M. F. W. C. (2010). Rapid, high sensitivity, point-of-care test for cardiac troponin based on optomagnetic biosensor. *Clinica Chimica Acta, 411*, 868–873.

Dong, L., Agarwal, A. K., Beebe, D. J., & Jiang, H. (2006). Adaptive liquid microlenses activated by stimuli-responsive hydrogels. *Nature, 442*, 551–554.

Duffy, D. C., McDonald, J. C., Schueller, O. J. A., & Whitesides, G. M. (1998). Rapid prototyping of microfluidic systems in poly(dimethylsiloxane). *Analytical Chemistry, 70*, 4974–4984.

Erickson, D., Sinton, D., & Psaltis, D. (2011). Optofluidics for energy applications. *Nature Photonics, 5*, 583–590.

Fan, X., & White, I. M. (2011). Optofluidic microsystems for chemical and biological analysis. *Nature Photonics, 5*, 591–597.

Fan, X., White, I. M., Shopova, S. I., Zhu, H., Suter, J. D., & Sun, Y. (2008). Sensitive optical biosensors for unlabeled targets: A review. *Analytica Chimica Acta, 620*, 8–26.

Fang, N., Lee, H., Sun, C., & Zhang, X. (2005). Sub-diffraction-limited optical imaging with a silver superlens. *Science, 308*, 534–537.

Fang, C., Dai, B., Xu, Q., Zhuo, R., Wang, Q., Wang, X., & Zhang, D. (2017). Hydrodynamically reconfigurable optofluidic microlens with continuous shape tuning from biconvex to biconcave. *Optics Express, 25*, 888–897.

Gattass, R. R., & Mazur, E. (2008). Femtosecond laser micromachining in transparent materials. *Nature Photonics, 2*, 219–225.

Gérard, D., Wenger, J., Devilez, A., Gachet, D., Stout, B., Bonod, N., Popov, E., & Rigneault, H. (2008). Strong electromagnetic confinement near dielectric microspheres to enhance single-molecule fluorescence. *Optics Express, 16*, 15297–15303.

Godin, J., Chen, C.-H., Cho, S. H., Qiao, W., Tsai, F., & Lo, Y.-H. (2008). Microfluidics and photonics for bio-system-on-a-Chip: A review of advancements in technology towards a microfluidic flow cytometry chip. *Journal of Biophotonics, 1*, 355–376.

Greenbaum, A., Luo, W., Su, T.-W., Göröcs, Z., Xue, L., Isikman, S. O., Coskun, A. F., Mudanyali, O., & Ozcan, A. (2012). Imaging without lenses: Achievements and remaining challenges of wide-field on-chip microscopy. *Nature Methods, 9*, 889–895.

Guo, F., Lapsley, M. I., Nawaz, A. A., Zhao, Y., Lin, S.-C. S., Chen, Y., Yang, S., Zhao, X.-Z., & Huang, T. J. (2012). A droplet-based, optofluidic device for high-throughput, quantitative bioanalysis. *Analytical Chemistry, 84*, 10745–10749.

Gupta, R., & Goddard, N. J. (2013). A novel leaky waveguide grating (LWG) device for evanescent wave broadband absorption spectroscopy in microfluidic flow cells. *Analyst, 138*, 1803–1811.

Haeberle, S., & Zengerle, R. (2007). Microfluidic platforms for lab-on-a-chip applications. *Lab on a Chip, 7*, 1094–1110.

Hamburg, M. A., & Collins, F. S. (2010). The path to personalized medicine. *The New England Journal of Medicine, 363*, 301–304.

Hanumegowda, N. M., Stica, C. J., Patel, B. C., White, I., & Fan, X. (2005). Refractometric sensors based on microsphere resonators. *Applied Physics Letters, 87*, 201107.

Harrick, N. J. (1962). Use of frustrated total internal reflection to measure film thickness and surface reliefs. *Journal of Applied Physics, 33*, 2774–2775.

Hawkins, A. R., & Schmidt, H. (2008). Optofluidic waveguides: II. Fabrication and structures. *Microfluidics and Nanofluidics, 4*, 17–32.

Heifetz, A., Kong, S.-C., Sahakian, A. V., Taflove, A., & Backman, V. (2009). Photonic nanojets. *Journal of Computational and Theoretical Nanoscience, 6*, 1979–1992.

Helmerhorst, E., Chandler, D. J., Nussio, M., & Mamotte, C. D. (2012). Real-time and label-free bio-sensing of molecular interactions by surface plasmon resonance: A laboratory medicine perspective. *Clinical Biochemist Reviews, 33*, 161–173.

Hofmann, O., Miller, P., Sullivan, P., Jones, T. S., de Mello, J. C., Bradley, D. D. C., & de Mello, A. J. (2005). Thin-film organic photodiodes as integrated detectors for microscale chemiluminescence assays. *Sensors and Actuators B: Chemical, 106*, 878–884.

Hu, Y., Rao, S., Wu, S., Wei, P., Qiu, W., Wu, D., Xu, B., Ni, J., Yang, L., Li, J., Chu, J., & Sugioka, K. (2018). All-glass 3D optofluidic microchip with built-in tunable microlens fabricated by femtosecond laser-assisted etching. *Advanced Optical Materials, 6*, 1701299.

Huang, P.-H., Lapsley, M. I., Ahmed, D., Chen, Y., Wang, L., & Huang, T. J. (2012). A single-layer, planar, optofluidic switch powered by acoustically driven, oscillating microbubbles. *Applied Physics Letters, 101*, 141101.

Huang, N.-T., Zhang, H.-L., Chung, M.-T., Seo, J. H., & Kurabayashi, K. (2014). Recent advancements in optofluidics-based single-cell analysis: Optical on-chip cellular manipulation, treatment, and property detection. *Lab on a Chip, 14*, 1230–1245.

Ibarlucea, B., Fernandez-Rosas, E., Vila-Planas, J., Demming, S., Nogúes, C., Plaza, J. A., Büttgenbach, S., & Llobera, A. (2010). Cell screening using disposable photonic lab on a chip systems. *Analytical Chemistry, 82*, 4246–4251.

Jiang, X., Song, Q., Xu, L., Fu, J., & Tong, L. (2007). Microfiber knot dye laser based on the evanescent-wave-coupled gain. *Applied Physics Letters, 90*, 233501.

Jung, K.-H., & Lee, K.-H. (2015). Molecular imaging in the era of personalized medicine. *Journal of Pathology and Translational Medicine, 49*, 5–12.

Kamei, T., Paegel, B. M., Scherer, J. R., Skelley, A. M., Street, R. A., & Mathies, R. A. (2003). Integrated hydrogenated amorphous Si photodiode detector for microfluidic bioanalytical devices. *Analytical Chemistry, 75*, 5300–5305.

Kasahara, T., Matsunami, S., Edura, T., Oshima, J., Adachi, C., Shoji, S., & Mizuno, J. (2013). Fabrication and performance evaluation of microfluidic organic light emitting diode. *Sensors and Actuators A, 195*, 219–223.

Kemmler, M., Koger, B., Sulz, G., Sauer, U., Schleicher, E., Preininger, C., & Brandenburg, A. (2009). Compact point-of-care system for clinical diagnostics. *Sensors and Actuators B: Chemical, 139*, 44–51.

Kopp, D., Lehmann, L., & Zappe, H. (2016). Optofluidic laser scanner based on a rotating liquid prism. *Applied Optics, 55*, 2136–2142.

Lee, H., Liu, Y., Ham, D., & Westervelt, R. M. (2007). Integrated cell manipulation system—CMOS/microfluidic hybrid. *Lab on a Chip, 7*, 331–337.
Lee, K. S., Kim, S. B., Lee, K. H., Sung, H. J., & Kim, S. S. (2010). Three-dimensional microfluidic liquid-core/liquid-cladding waveguide. *Applied Physics Letters, 97*, 021109.
Lee, W., Li, H., Suter, J. D., Reddy, K., Sun, Y., & Fan, X. (2011). Tunable single mode lasing from an on-chip optofluidic ring resonator laser. *Applied Physics Letters, 98*, 061103.
Li, D. (Ed.). (2015a). *Encyclopedia of microfluidics and nanofluidics* (pp. 2109–2114). Springer.
Li, D. (Ed.). (2015b). *Encyclopedia of microfluidics and nanofluidics* (pp. 2089–2090). Springer.
Li, Z., & Psaltis, D. (2008). Optofluidic dye lasers. *Microfluidics and Nanofluidics, 4*, 145–158.
Li, X., Chen, Z., Taflove, A., & Backman, V. (2005). Optical analysis of nanoparticles via enhanced backscattering facilitated by 3-D photonic nanojets. *Optics Express, 13*, 526–533.
Li, L., Guo, W., Yan, Y., Lee, S., & Wang, T. (2013). Label-free super-resolution imaging of adenoviruses by submerged microsphere optical nanoscopy. *Light: Science and Applications, 2*, e104.
Li, Y., Liu, X., Yang, X., Lei, H., Zhang, Y., & Li, B. (2017). Enhancing upconversion fluorescence with a natural bio-microlens. *ACS Nano, 11*, 10672–10680.
Liang, X. J., Liu, A. Q., Lim, C. S., Ayi, T. C., & Yap, P. H. (2007). Determining refractive index of single living cell using an integrated microchip. *Sensors and Actuators A, 133*, 349–354.
Liu, H., Shi, Y., Liang, L., Li, L., Guo, S., Yin, L., & Yang, Y. (2017a). A liquid thermal gradient refractive index lens and using it to trap single living cell in flowing environments. *Lab on a Chip, 17*, 1280–1286.
Liu, L., Zhou, X., Lu, M., Zhang, M., Yang, C., Ma, R., Memon, A. G., Shi, H., & Qian, Y. (2017b). An array fluorescent biosensor based on planar waveguide for multi-analyte determination in water samples. *Sensors and Actuators B: Chemical, 240*, 107–113.
Manz, A., Graber, N., & Widmer, H. M. (1990). Miniaturized total chemical analysis systems: A novel concept for chemical sensing. *Sensors and Actuators B: Chemical, 1*, 244–248.
Mao, X., Waldeisen, J. R., Juluri, B. K., & Huang, T. J. (2007). Hydrodynamically tunable optofluidic cylindrical microlens. *Lab on a Chip, 7*, 1303–1308.
Mao, X., Lin, S.-C. S., Lapsley, M. I., Shi, J., Juluri, B. K., & Huang, T. J. (2009). Tunable liquid gradient refractive index (L-GRIN) lens with two degrees of freedom. *Lab on a Chip, 9*, 2050–2058.
Mark, D., Haeberle, S., Roth, G., Stetten, F. V., & Zengerle, R. (2010). Microfluidic lab-on-a-chip platforms: requirements, characteristics and applications. *Chemical Society Reviews, 39*, 1153–1182.
McLeod, E., & Arnold, C. B. (2008). Subwavelength direct-write nanopatterning using optically trapped microspheres. *Nature Nanotechnology, 3*, 413–417.
Miccio, L., Memmolo, P., Merola, F., Netti, P. A., & Ferraro, P. (2015). Red blood cell as an adaptive optofluidic microlens. *Nature Communications, 6*, 6502.
Minzioni, P., Osellame, R., Sada, C., Zhao, S., Omenetto, F., Gylfason, K. B., Haraldsson, T., Zhang, Y., Ozcan, A., Wax, A., Mugele, F., Schmidt, H., Testa, G., Bernini, R., Guck, J., Liberale, C., Berg-Sørensen, K., Chen, J., Pollnau, M., Xiong, S., Liu, A.-Q., Shiue, C.-C., Fan, S.-K., Erickson, D., & Sinton, D. (2017). Roadmap for optofluidics. *Journal of Optics, 19*, 093003.
Mishra, K., Murade, C., Carreel, B., Roghair, I., Oh, J. M., Manukyan, G., van den Ende, D., & Mugele, F. (2014). Optofluidic lens with tunable focal length and asphericity. *Scientific Reports, 4*, 6378.
Mohammed, M.-I., & Desmulliez, M. P. Y. (2013). Planar lens integrated capillary action microfluidic immunoassay device for the optical detection of troponin I. *Biomicrofluidics, 7*, 064112.
Monat, C., Domachuk, P., & Eggleton, B. J. (2007). Integrated optofluidics: A new river of light. *Nature Photonics, 1*, 106–114.
Monks, J. N., Yan, B., Hawkins, N., Vollrath, F., & Wang, Z. (2016). Spider silk: Mother nature's bio-superlens. *Nano Letters, 16*, 5842–5845.

Muñoz-Berbel, X., Rodríguez-Rodríguez, R., Vigués, N., Demming, S., Mas, J., Büttgenbach, S., Verpoorte, E., Ortiz, P., & Llobera, A. (2013). Monolithically integrated biophotonic lab-on-a-chip for cell culture and simultaneous pH monitoring. *Lab on a Chip, 13*, 4239–4247.

Nguyen, N.-T. (2010). Micro-optofluidic lenses: A review. *Biomicrofluidics, 4*, 031501.

Ozcan, A., & McLeod, E. (2016). Lensless imaging and sensing. *Annual Review of Biomedical Engineering, 18*, 77–102.

Pang, L., Chen, H. M., Freeman, L. M., & Fainman, Y. (2012). Optofluidic devices and applications in photonics, sensing and imaging. *Lab on a Chip, 12*, 3543–3551.

Pendry, J. B. (2000). Negative refraction makes a perfect lens. *Physical Review Letters, 85*, 3966–3969.

Piyasena, M. E., & Graves, S. W. (2014). The intersection of flow cytometry with microfluidics and microfabrication. *Lab on a Chip, 14*, 1044–1059.

Ro, K. W., Lim, K., Shim, B. C., & Hahn, J. H. (2005). Integrated light collimating system for extended optical-path-length absorbance detection in microchip-based capillary electrophoresis. *Analytical Chemistry, 77*, 5160–5166.

Rodríguez-Ruiz, I., Ackermann, T. N., Muñoz-Berbel, X., & Llobera, A. (2016). Photonic lab-on-a-chip: Integration of optical spectroscopy in microfluidic systems. *Analytical Chemistry, 88*, 6630–6637.

Rosenauer, M., & Vellekoop, M. J. (2009a). A versatile liquid-core/liquid-twin-cladding waveguide micro flow cell fabricated by rapid prototyping. *Applied Physics Letters, 95*, 163702.

Rosenauer, M., & Vellekoop, M. J. (2009b). 3D fluidic lens shaping—A multiconvex hydrodynamically adjustable optofluidic microlens. *Lab on a Chip, 9*, 1040–1042.

Schmidt, H., & Hawkins, A. R. (2008). Optofluidic waveguides: I. concepts and implementations. *Microfluidics and Nanofluidics, 4*, 3–16.

Schmidt, H., & Hawkins, A. R. (2011). The photonic integration of non-solid media using optofluidics. *Nature Photonics, 5*, 598–604.

Schuergers, N., Lenn, T., Kampmann, R., Meissner, M. V., Esteves, T., Temerinac-Ott, M., Korvink, J. G., Lowe, A. R., Mullineaux, C. W., & Wilde, A. (2016). Cyanobacteria use micro-optics to sense light direction. *eLife, 5*, e12620.

Schwartz, J. J., Stavrakis, S., & Quake, S. R. (2010). Colloidal lenses allow high-temperature single-molecule imaging and improve fluorophore photostability. *Nature Nanotechnology, 5*, 127–132.

Seo, J., & Lee, L. P. (2004). Disposable integrated microfluidics with self-aligned planar microlenses. *Sensors and Actuators B: Chemical, 99*, 615–622.

Seo, S., Su, T.-W., Tseng, D. K., Erlinger, A., & Ozcan, A. (2009). Lensfree holographic imaging for on-chip cytometry and diagnostics. *Lab on a Chip, 9*, 777–787.

Shi, J., Stratton, Z., Lin, S.-C. S., Huang, H., & Huang, T. J. (2010). Tunable optofluidic microlens through active pressure control of an air–liquid interface. *Microfluidics and Nanofluidics, 9*, 313–318.

Shopova, S. I., Zhou, H., Fan, X., & Zhang, P. (2007). Optofluidic ring resonator based dye laser. *Applied Physics Letters, 90*, 221101.

Song, C., & Tan, S. H. (2017). A perspective on the rise of optofluidics and the future. *Micromachines, 8*, 152.

Song, W., Vasdekis, A. E., Li, Z., & Psaltis, D. (2009). Optofluidic evanescent dye laser based on a distributed feedback circular grating. *Applied Physics Letters, 94*, 161110.

Song, C., Nguyen, N.-T., Tan, S.-H., & Asundi, A. K. (2010). A tuneable micro-optofluidic biconvex lens with mathematically predictable focal length. *Microfluidics and Nanofluidics, 9*, 889–896.

Song, C., Nguyen, N.-T., Yap, Y. F., Luong, T.-D., & Asundi, A. K. (2011). Multi-functional, optofluidic, in-plane, bi-concave lens: Tuning light beam from focused to divergent. *Microfluidics and Nanofluidics, 10*, 671–678.

Tang, S. K., Li, Z., Abate, A. R., Agresti, J. J., Weitz, D. A., Psaltis, D., & Whitesides, G. M. (2009). A multi-color fast-switching microfluidic droplet dye laser. *Lab on a Chip, 9*, 2767–2771.

Testa, G., Huang, Y., Zeni, L., Sarro, P. M., & Bernini, R. (2010). Liquid core ARROW waveguides by atomic layer deposition. *IEEE Photonics Technology Letters, 22*, 616–618.

Threm, D., Nazirizadeh, Y., & Gerken, M. (2012). Photonic crystal biosensors towards on-chip integration. *Journal of Biophotonics, 5*, 601–616.

Tung, Y.-C., Huang, N.-T., Oh, B.-R., Patra, B., Pan, C.-C., Qiu, T., Chu, P. K., Zhang, W., & Kurabayashi, K. (2012). Optofluidic detection for cellular phenotyping. *Lab on a Chip, 12*, 3552–3565.

Vezenov, D. V., Mayers, B. T., Conroy, R. S., Whitesides, G. M., Snee, P. T., Chan, Y., Nocera, D. G., & Bawendi, M. G. (2005). A low-threshold, high-efficiency microfluidic waveguide laser. *Journal of the American Chemical Society, 127*, 8952–8953.

Vila-Planas, J., Fernandez-Rosas, E., Ibarlucea, B., Demming, S., Nogúes, C., Plaza, J. A., Domínguez, C., Büttgenbach, S., & Llobera, A. (2011). Cell analysis using a multiple internal reflection photonic lab-on-a-chip. *Nature Protocols, 6*, 1642–1655.

Wang, Z., Guo, W., Li, L., Luk'yanchuk, B., Khan, A., Liu, Z., Chen, Z., & Hong, M. (2011). Optical virtual imaging at 50 nm lateral resolution with a white-light nanoscope. *Nature Communications, 2*, 218.

Watts, B. R., Kowpak, T., Zhang, Z., Xu, C.-Q., & Zhu, S. (2010). Formation and characterization of an ideal excitation beam geometry in an optofluidic device. *Biomedical Optics Express, 1*, 848–860.

Watts, B. R., Zhang, Z., Xu, C.-Q., Cao, X., & Lin, M. (2013). A method for detecting forward scattering signals on-chip with a photonic-microfluidic integrated device. *Biomedical Optics Express, 4*, 1051–1060.

Wei, Q., McLeod, E., Qi, H., Wan, Z., Sun, R., & Ozcan, A. (2013). On-chip cytometry using plasmonic nanoparticle enhanced lensfree holography. *Scientific Reports, 3*, 1699.

Wojciechowski, J. R., Shriver-Lake, L. C., Yamaguchi, M. Y., Füreder, E., Pieler, R., Schamesberger, M., Winder, C., Prall, H. J., Sonnleitner, M., & Ligler, F. S. (2009). Organic photodiodes for biosensor miniaturization. *Analytical Chemistry, 81*, 3455–3461.

Wolfe, D. B., Conroy, R. S., Garstecki, P., Mayers, B. T., Fischbach, M. A., Paul, K. E., Prentiss, M., & Whitesides, G. M. (2004). Dynamic control of liquid-core/liquid-cladding optical waveguides. *Proceedings of the National Academy of Sciences of the United States of America, 101*, 12434–12438.

Wolfe, D. B., Vezenov, D. V., Mayers, B. T., Whitesides, G. M., Conroy, R. S., & Prentiss, M. G. (2005). Diffusion-controlled optical elements for optofluidics. *Applied Physics Letters, 87*, 181105.

Wu, J., & Gu, M. (2011). Microfluidic sensing: State of the art fabrication and detection techniques. *Journal of Biomedical Optics, 16*, 080901.

Wynne, T. M., Dixon, A. H., & Pennathur, S. (2012). Electrokinetic characterization of individual nanoparticles in nanofluidic channels. *Microfluidics and Nanofluidics, 12*, 411–421.

Xiong, S., Liu, A., Chin, L., & Yang, Y. (2011). An optofluidic prism tuned by two laminar flows. *Lab on a Chip, 11*, 1864–1869.

Xu, D., & Adachi, C. (2009). Organic light-emitting diode with liquid emitting layer. *Applied Physics Letters, 95*, 053304.

Yan, Y., Li, L., Feng, C., Guo, W., Lee, S., & Hong, M. (2015). Microsphere-coupled scanning laser confocal nanoscope for sub-diffraction-limited imaging at 25 nm lateral resolution in the visible spectrum. *ACS Nano, 8*, 1809–1816.

Yang, H., & Gijs, M. A. M. (2013). Microtextured substrates and microparticles used as in situ lenses for on-chip immunofluorescence amplification. *Analytical Chemistry, 85*, 2064–2071.

Yang, H., & Gijs, M. A. M. (2015). Optical microscopy using a glass microsphere for metrology of sub-wavelength nanostructures. *Microelectronic Engineering, 143*, 86–90.

Yang, H., & Gijs, M. A. M. (2018). Micro-optics for microfluidic analytical applications. *Chemical Society Reviews, 47*, 1391–1458.

Yang, H., Chao, C.-K., Lin, C.-P., & Shen, S.-C. (2004). Micro-ball lens array modeling and fabrication using thermal reflow in two polymer layers. *Journal of Micromechanics and Microengineering, 14*, 277–282.

Yang, H., Moullan, N., Auwerx, J., & Gijs, M. A. M. (2014). Super-resolution biological microscopy using virtual imaging by a microsphere nanoscope. *Small, 10*, 1712–1718.

Yang, H., Cornaglia, M., & Gijs, M. A. M. (2015). Photonic nanojet array for fast detection of single nanoparticles in a flow. *Nano Letters, 15*, 1730–1735.

Yang, H., Trouillon, R., Huszka, G., & Gijs, M. A. M. (2016a). Super-resolution imaging of a dielectric microsphere is governed by the waist of its photonic nanojet. *Nano Letters, 16*, 4862–4870.

Yang, T., Bragheri, F., & Minzioni, P. (2016b). A comprehensive review of optical stretcher for cell mechanical characterization at single-cell level. *Micromachines, 7*, 90.

Yang, H., Zhang, Y., Chen, S., & Hao, R. (2019). Micro-optical components for bioimaging on tissues, cells and subcellular structures. *Micromachines, 10*, 405.

Yao, B., Luo, G., Wang, L., Gao, Y., Lei, G., Ren, K., Chen, L., Wang, Y., Hu, Y., & Qiu, Y. (2005). A microfluidic device using a green organic light emitting diode as an integrated excitation source. *Lab on a Chip, 5*, 1041–1047.

Yu, H., Zhou, G., Leung, H. M., & Chau, F. S. (2010). Tunable liquid-filled lens integrated with aspherical surface for spherical aberration compensation. *Optics Express, 18*, 9945–9954.

Zhang, H., Ho, S., Eaton, S. M., Li, J., & Herman, P. R. (2008). Three-dimensional optical sensing network written in fused silica glass with femtosecond laser. *Optics Express, 16*, 14015–14023.

Zhao, Y., Zhao, X., & Gu, Z. (2010). Photonic crystals in bioassays. *Advanced Functional Materials, 20*, 2970–2988.

Zhao, Y., Stratton, Z. S., Guo, F., Lapsley, M. I., Chan, C. Y., Lin, S.-C. S., & Huang, T. J. (2013). Optofluidic imaging: Now and beyond. *Lab on a Chip, 13*, 17–24.

Zheng, H. Y., Liu, H., Wan, S., Lim, G. C., Nikumb, S., & Chen, Q. (2006). Ultrashort pulse laser micromachined microchannels and their application in an optical switch. *International Journal of Advanced Design and Manufacturing Technology, 27*, 925–929.

Zhu, H., Mavandadi, S., Coskun, A. F., Yaglidere, O., & Ozcan, A. (2011). Optofluidic fluorescent imaging cytometry on a cell phone. *Analytical Chemistry, 83*, 6641–6647.